Volume 53
Number 22
21 November 2024
Pages 10793–11252

Chem Soc Rev

Chemical Society Reviews

rsc.li/chem-soc-rev

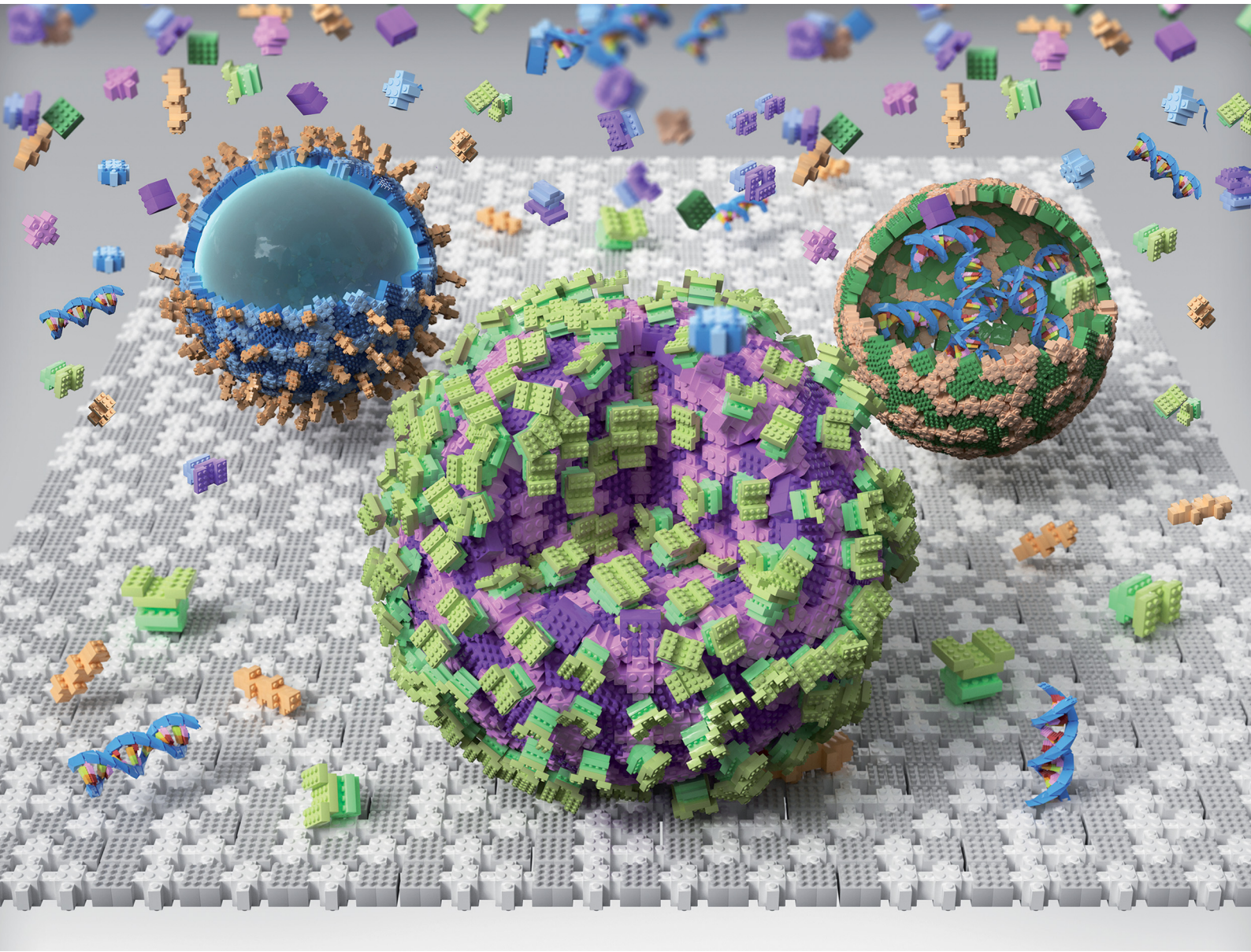

ISSN 0306-0012

ROYAL SOCIETY OF CHEMISTRY

TUTORIAL REVIEW

Frank Caruso, Jiajing Zhou *et al.*

Metal–phenolic network composites: from fundamentals to applications

Chem Soc Rev

TUTORIAL REVIEW

View Article Online
View Journal | View Issue

Cite this: *Chem. Soc. Rev.*, 2024, **53**, 10800

Metal–phenolic network composites: from fundamentals to applications

Zhixing Lin, †[a] Hai Liu, †[b] Joseph J. Richardson,[c] Wanjun Xu,[a] Jingqu Chen,[a] Jiajing Zhou *[b] and Frank Caruso *[a]

Composites with tailored compositions and functions have attracted widespread scientific and industrial interest. Metal–phenolic networks (MPNs), which are composed of phenolic ligands and metal ions, are amorphous adhesive coordination polymers that have been combined with various functional components to create composites with potential in chemistry, biology, and materials science. This review aims to provide a comprehensive summary of both fundamental knowledge and advancements in the field of MPN composites. The advantages of amorphous MPNs, over crystalline metal–organic frameworks, for fabricating composites are highlighted, including their mild synthesis, diverse interactions, and numerous intrinsic functionalities. The formation mechanisms and state-of-the-art synthesis strategies of MPN composites are summarized to guide their rational design. Subsequently, a detailed overview of the chemical interactions and structure–property relationships of composites based on different functional components (*e.g.*, small molecules, polymers, biomacromolecules) is provided. Finally, perspectives are offered on the current challenges and future directions of MPN composites. This tutorial review is expected to serve as a fundamental guide for researchers in the field of metal–organic materials and to provide insights and avenues to enhance the performance of existing functional materials in applications across diverse fields.

Received 4th June 2024

DOI: 10.1039/d3cs00273j

rsc.li/chem-soc-rev

Key learning points
(1) Advantages and challenges of using MPNs for fabricating composites.
(2) Synthesis strategies for MPN composites.
(3) Fundamental interactions between MPNs and different functional components.
(4) Synergistic effects of MPNs and functional components for specific applications.
(5) Future challenges and opportunities for MPN composites.

1. Introduction

Functional composites with tailored properties play a pivotal role in fundamental studies and translational applications in diverse disciplines, including chemistry, biology, and materials science.[1–3] Pristine materials allow for detailed fundamental studies, whereas composite materials, where functional materials (*e.g.*, nanoparticle, protein, polymer) can be embedded in or incorporated throughout another material, can be engineered to display a range of desired functionalities. For example, pristine metal–organic frameworks (MOFs), which are composed of organic ligands and metal ions or clusters, are of scientific interest owing to their physiochemical properties,[4–6] although the functionalities of MOFs can be restricted by the ligands applicable to their synthesis. Therefore, various functional components (*e.g.*, proteins and nanoparticles) with distinct properties have been incorporated into MOFs to create composite materials with desirable functions for various applications.[7–9] However, the integration of functional components within these crystalline materials is typically restricted by the pore size of the MOFs, specific covalent interactions, or complex postsynthetic strategies.[10–13] These, in turn, limit the type of cargo and the functionality of the resultant metal–organic composites with regard to emerging applications.

[a] *Department of Chemical Engineering, The University of Melbourne, Parkville, Victoria, 3010, Australia. E-mail: fcaruso@unimelb.edu.au*
[b] *College of Biomass Science and Engineering, Sichuan University, Chengdu, Sichuan, 610065, China. E-mail: jjzhou@scu.edu.cn*
[c] *School of Engineering, RMIT University, Melbourne, Victoria, 3000, Australia*
† Z. L. and H. L. contributed equally to this work.

Metal–phenolic networks (MPNs) are amorphous coordination networks composed of metal ions and phenolic ligands.[14–17] The presence of phenolic catechol and gallol groups enables MPNs to interact with various functional components *via* a range of interactions (*e.g.*, hydrogen bonding, π interactions, hydrophobic interactions).[18–20] Therefore, diverse MPN composites—formulated by combining MPNs and one or more functional components (*e.g.*, drugs, proteins, and nanoparticles)—have been developed and applied across diverse applications, including separations, energy storage, drug delivery, catalysis, and bioimaging.[21–23] Moreover, the inherent properties of MPNs (*e.g.*, high porosity, pH responsiveness, and metal-dependent functionality) can be incorporated into composites to enhance the performance of other functional components.[24] MPN composite materials have undergone rapid development in the last decade since the first report in 2013[14] and have potential applications in a wide range of fields, including chemistry, biology, and materials science.[15,17,18] A comprehensive review summarizing the fundamental mechanisms, synthetic strategies, and properties of MPN composites is expected to significantly bridge knowledge gaps, inspire innovative approaches in synthesizing MPN composites, and catalyze new research directions for diverse scientific and industrial applications.

In this tutorial review, we cover the fundamentals of MPN composites and highlight the significant progress made to date to guide future directions in the field (Fig. 1). We first introduce the advantages of using molecular building blocks and the physicochemical properties of MPNs that make them useful for fabricating composites (Section 2). We then summarize state-of-the-art strategies for preparing MPN composites (Section 3), followed by a detailed overview of the chemical interactions and structure–property relationships of composites based on the different functional components, including small molecules, polymers, biomacromolecules, metal nanoparticles, oxides, biological entities, and other functional materials (Section 4). Finally,

Zhixing Lin

Zhixing Lin received his Master's degree from Shanghai Jiao Tong University and his PhD in Chemical and Biomolecular Engineering in 2021 under the supervision of Prof. Frank Caruso at The University of Melbourne. He is currently a Senior Research Fellow in Prof. Caruso's group. His research interests focus on understanding and controlling the relationships between the composition, structure, and performance of metal–organic materials at the nanoscale, with applications across the environmental, agricultural, and biomedical sciences.

Hai Liu

Hai Liu is a PhD student in the College of Biomass Science and Engineering at Sichuan University under the supervision of Prof. Jiajing Zhou and Prof. Wei Lin. He received his BS degree from Jiangnan University. His current research work focuses on phenolic-enabled nanotechnology, biohybrid materials, and 3D bioprinting.

Joseph J. Richardson

Joseph J. (JJ) Richardson was born in the sunshine state of the USA, Florida. He pursued his BA in Philosophy and MS in Industrial and Systems Engineering at the University of Florida and completed his PhD in Chemical and Biomolecular Engineering under the supervision of Prof. Frank Caruso at The University of Melbourne. JJ has lived and worked in seven countries and his research lies at the interface of nanomaterials and biological systems. His current focus as an ARC Future Fellow at RMIT University is on the application of nanomaterials to biotechnology challenges in health and the environment.

Wanjun Xu

Wanjun Xu received her PhD in 2023 from the School of Chemical and Biomedical Engineering at The University of Melbourne, under the supervision of Prof. Frank Caruso. She is currently a Research Fellow in the same group and her research interests focus on understanding and regulating the assembly of metal–organic materials at the molecular level and expanding the realm of metal–organic materials by endowing them with new properties for various applications.

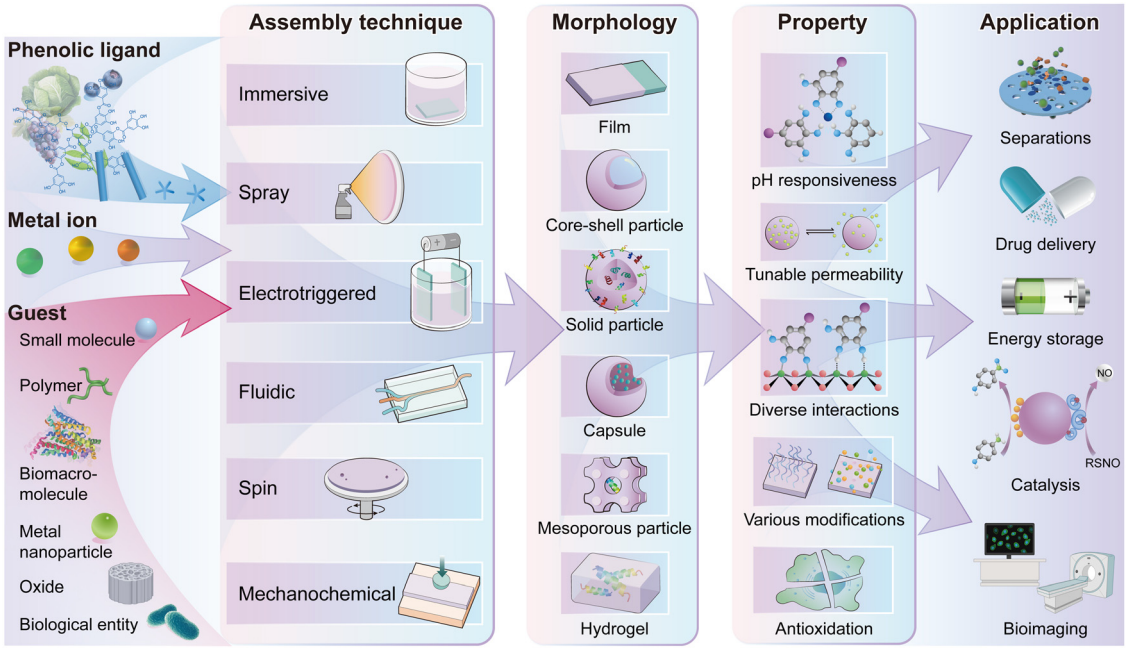

Fig. 1 Schematic illustration of the building blocks, assembly techniques, morphologies, properties and applications of MPN composites.

we offer a perspective on the future challenges, opportunities, and directions related to the field of MPN composites (Section 5). This tutorial review is expected to serve as a guide for researchers in the field of functional composite metal–organic materials.

2. Engineered MPNs to fabricate composites

In this section, we introduce the building blocks involved in the fabrication of MPNs and the advantages of coupling these building blocks with a functional component to prepare MPN composites.

2.1. MPN molecular building blocks

2.1.1. Phenolic ligands. The molecular building blocks of MPNs are both widespread and modular, with phenolic ligands alone comprising over 8000 distinct molecules found in nature and a nearly limitless number of theoretical synthetic ligands (Fig. 2).[25] Notably, phenolic ligands are naturally prevalent in fruits (*e.g.*, blueberries, grapes), nuts (*e.g.*, hazelnuts, walnuts), and tree leaves (*e.g.*, *Pinus pinaster*), as well as various vegetables (*e.g.*, onions, bell peppers) (Fig. 2a).[26] Moreover, natural

Jiajing Zhou

Jiajing Zhou completed his PhD in Bioengineering in 2016 from Nanyang Technological University under the supervision of Prof. Hongwei Duan. He conducted his postdoctoral research in Prof. Frank Caruso's group at The University of Melbourne from 2018 to 2020 and in Prof. Jesse Jokerst's group at the University of California San Diego from 2020 to 2022. Since 2022, he has been a professor in the College of Biomass Science and Engineering at Sichuan University. His research interests include biomass materials engineering and 3D bioprinting for biomedical and environmental applications.

Frank Caruso

Frank Caruso is a Melbourne Laureate Professor and an NHMRC Leadership Fellow at The University of Melbourne. He received his PhD in 1994 from The University of Melbourne and thereafter conducted postdoctoral research at CSIRO Division of Chemicals and Polymers. In 1997–2002, he was a Humboldt Research Fellow and Group Leader at the Max Planck Institute of Colloids and Interfaces (Germany). Since 2003, he has been a professor at The University of Melbourne and has held ARC Federation and ARC Australian Laureate Fellowships. His research interests focus on developing advanced nano- and biomaterials for biotechnology and medicine.

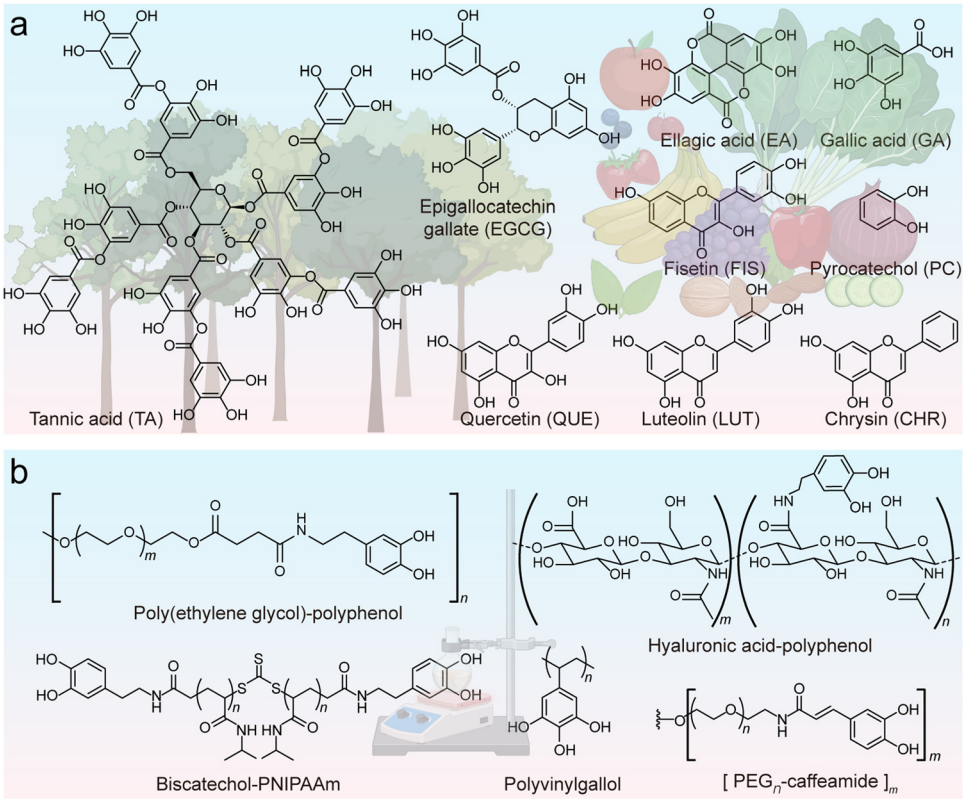

Fig. 2 Representative examples of (a) natural and (b) synthetic phenolic ligands.

polyphenols have found applications in both traditional and contemporary medicine, winemaking, rust mitigation in pipes, wastewater remediation, and historical practices such as iron-gall ink production.[27–29] Polyphenols have a variety of applications in nature and industry owing to their diverse physicochemical and biological properties that naturally benefit organisms, including UV absorption, reactive oxygen species (ROS) scavenging, antioxidation, and therapeutic efficacy.[26,30,31]

Additionally, the functionality of phenolic ligands can be tailored through modification with specific molecules (*e.g.*, hyaluronic acid (HA)-based phenolic ligands for cell targeting, Fig. 2b), and non-canonical phenolics can even be synthesized to unlock further properties such as high underwater adhesion.[32,33] For example, dopamine is commonly used to impart various molecules with catechol groups through amide coupling, succinimidyl succinate or carbodiimide coupling reactions.[20,34,35] Alternatively, more sophisticated approaches can be used to copolymerize phenolic polymers or create dendritic phenolic molecules with controllable size, length, and hydroxy number.[36,37] It is notable that the protection/deprotection of phenolic groups may be required in this process to avoid undesirable potential side reactions.[38] These synthetic polyphenols generally retain their physicochemical properties and ability to coordinate metal ions. For instance, cargo-loaded MPN composites with adjustable cell-targeting efficacy were prepared by altering the ratio of dopamine-modified polymeric phenolic ligands, including cell-targeting HA and low-fouling poly(ethylene glycol) (PEG).[32] Moreover, synthetic approaches allow for the formation of phenolic molecules not accessible to biological processes (*e.g.*, phenolic moieties with four or five hydroxy groups) that allow for the formation of advanced materials for specific applications.[33]

An important property of phenolics is their universal adhesion to substrates owing to their wide range of interactive forces (Fig. 3a–c).[14,18] Moreover, phenolic ligands can coordinate with a diverse array of metal ions without losing their adhesive nature, affording the generation of functional MPN coatings and materials. In this process, the hydroxy groups (–OH) of phenolics function as electron donors, whereas the metal ions, possessing vacant electron orbitals (known as coordination sites), accept electron pairs (Fig. 3d).[39] Thus, the hydroxy groups of the phenolic ligand can establish coordination bonds with the metal ions (Fig. 3e), enabling the mutual sharing of electron pairs between the metal ions and the oxygen atoms within the hydroxy groups and imparting stability to the resulting MPN coatings and materials.[39]

2.1.2. Metal ions. The formation of MPNs is a versatile and controllable process dependent on the incorporation of metal ions that holds significance in nature, particularly for plant pigmentation and cationic nutrient cycling, and in industry for energy, agriculture, and biomedicine.[17] Main group metal ions (*e.g.*, aluminum), transition metal ions (*e.g.*, iron, copper, cadmium), and lanthanide ions (*e.g.*, cerium, europium, samarium, and gadolinium) have been extensively used to fabricate

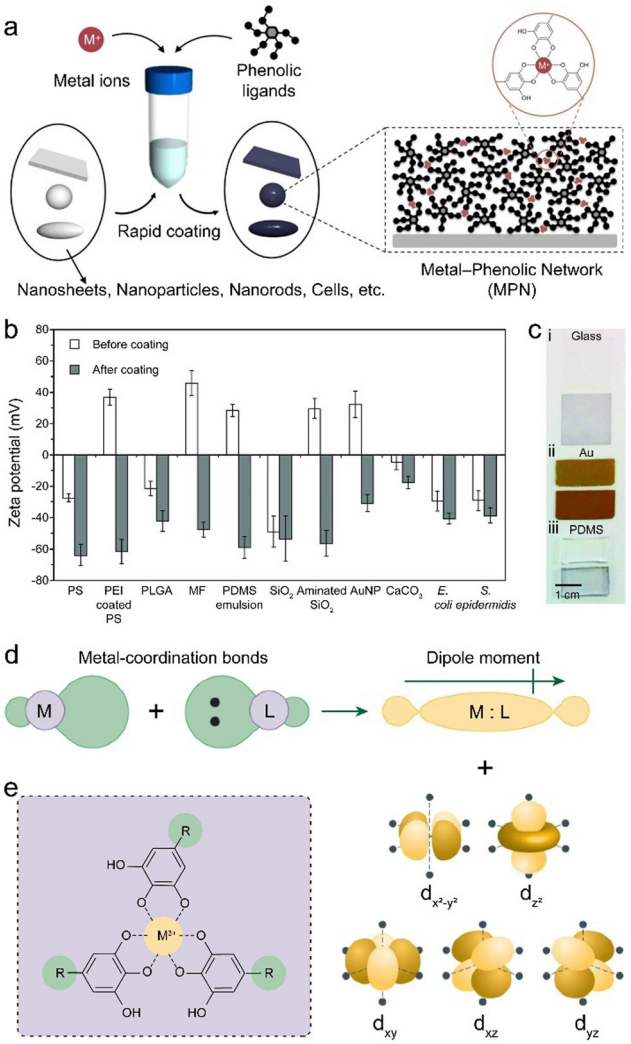

Fig. 3 (a) Schematic illustration of the rapid coating of MPNs on different substrates. (b) Zeta potential of the samples before and after the formation of MPN coatings. (c) Digital images of different samples before (upper) and after (lower) MPN coating. (a)–(c) Adapted with permission from ref. 14. Copyright 2013, The American Association for the Advancement of Science. (d) Schematic illustration of the formation of coordination bonds involving the donation of two electrons, generating molecular orbitals with a dipole moment and the distortion of the d orbitals of the metal ions. Adapted with permission from ref. 39. Copyright 2021, Springer Nature Limited. (e) Schematic illustration of the coordination between polyphenols and metal ions in MPNs.

MPNs (Fig. 4a).[24] MPNs exhibit various stoichiometries (*e.g.*, mono-, bis-, tris-complex) that can be modulated by various factors including pH, metal ion valency, or the molar ratio of metal ions to phenolic groups.[40] In turn, the species of metal ions and their related stoichiometries guide the properties of MPNs, such as film thickness, permeability, and disassembly. Moreover, the choice of metal ions can dictate the function of the MPNs.[17] For example, Rh^{3+}–tannic acid (TA) capsules have shown excellent catalytic properties for quinoline hydrogenation and Cu^{2+}–TA complexes serve as a positron emission tomography imaging probe.[24,41] Multimodal imaging and multicolor fluorescence is also achieved by incorporating multiple metals, providing an avenue for engineering multifunctional materials for various applications (Fig. 4b–d).[24,42] The distinct characteristics bestowed by metal ions offer versatility for preparing MPN composites, with potential application in various fields, including biomedicine, environmental remediation, and materials science.

2.2. Advantages of MPNs for constructing composites

Crystalline MOFs possess advantages that can benefit the fabrication of composites, which have been summarized in previous reviews.[7–13] However, MPNs possess some distinct advantages compared with crystalline MOFs for the formation of functional materials (Table 1).[15] For example, the mild synthesis conditions (*i.e.*, aqueous synthesis under ambient conditions) of MPNs can minimize the denaturation of bioactive functional components (*e.g.*, proteins), which benefits biomedical applications such as drug delivery.[43] Furthermore, various functional components (*e.g.*, drugs or proteins) can be easily pre- or postloaded into MPNs through diverse supramolecular interactions (*e.g.*, hydrogen bonding), which is a significant advantage over complex chemical conjugation routes and cargo size constraints typically associated with loading or functionalizing crystalline metal–organic materials. Moreover, functional phenolic ligands and/or metal ions can be readily incorporated into MPNs to provide new functionalities or enhance the performance of the other functional components. This section systematically discusses the benefits of using MPNs for fabricating composite materials.

2.2.1. Mild synthesis conditions. The assembly of MPNs is simple and facile: phenolic ligands and metal ions are assembled within minutes in aqueous solution at room temperature, eliminating the requirement for organic solvents and/or hydrothermal conditions that are typically used for the formation of crystalline metal–organic materials.[14,44] These mild synthesis conditions generally allow for the preservation of the activity of biological entities (*e.g.*, enzymes, yeast cells, and microalgae), thereby enabling the formation of biological composites particularly useful in biomedicine.[45] The mild synthesis conditions further enable the engineering of MPN composites *via* diverse assembly technologies (see Section 3.1 for details).

2.2.2. Diverse interactions with functional components. The broad adherence properties of phenolic ligands enable MPNs to interact with other materials through hydrogen bonding, π interactions, hydrophobic interactions, metal coordination, covalent bonding, and electrostatic interactions (Fig. 5a–k).[18,19] Therefore, a wide range of functional materials can directly interact with MPNs without a restrictive need on their chemical compositions, and many MPN composites are formed as a result of more than one type of stabilizing force but often with a dominant type of interaction.[46,47] To reveal their dominant interactions, a simplified system has been studied using TA and various proteins with different molecular weights, aliphatic indices, and charges.[21,48] The findings showed that hydrophobic interactions predominantly

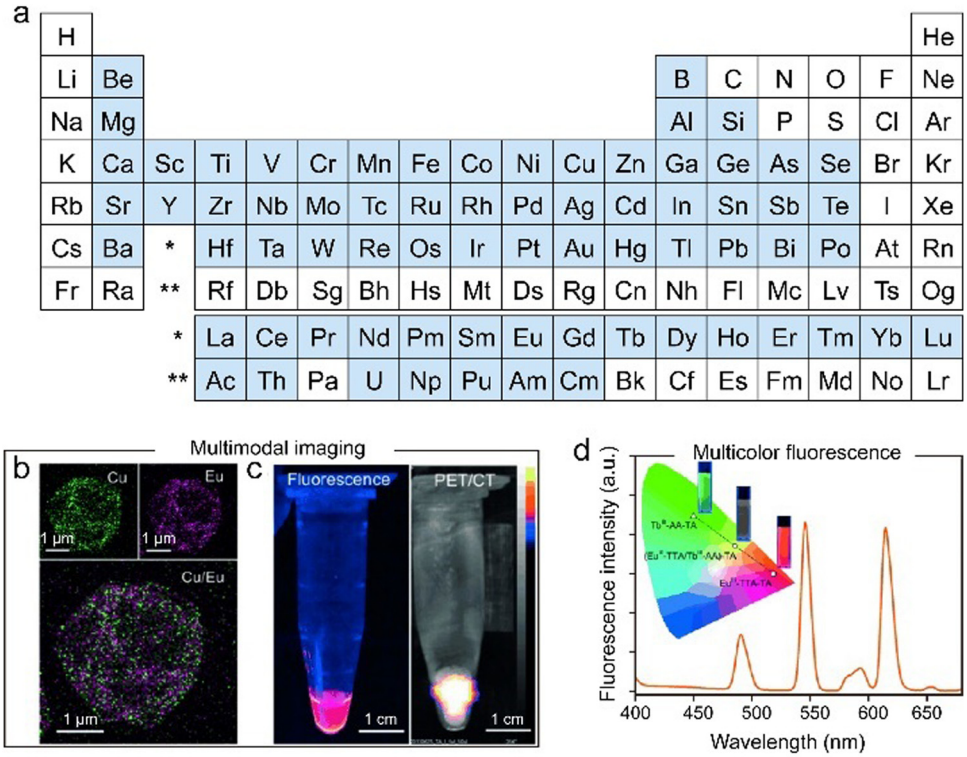

Fig. 4 (a) Assembly of MPNs from various metal ions. Metal ions highlighted in blue can be used to prepare MPN composites. Engineering multifunctional MPN capsules for (b) and (c) multimodal imaging and (d) multicolor fluorescence. (b)–(d) Adapted with permission from ref. 24. Copyright 2014, Wiley-VCH.

Table 1 Comparison of MPN composites and crystalline MOF composites[a]

	MPN composites	Crystalline MOF composites
Synthesis	Aqueous, simple, and relatively rapid process that preserves the activity of functional guests	Generally, requires specific solvents, pressure and temperature, and relatively slow process, guest molecules and cargo can expedite formation
	Mostly natural, flexible, and asymmetric ligands with relatively less control over side groups	Mostly rigid synthetic ligands with a high degree of synthetic control over side groups
	Generalized protocols	Metal-specific protocols
	Diverse assembly techniques	Material-specific techniques
Morphology	Amorphous structure	Defined crystalline structure
	Mostly spherical, but can be engineered into diverse morphologies (*e.g.*, anisotropic particles and films)	Typically, faceted polyhedral morphology
	Narrow size distribution	Controllable size distribution
	Easy to form conformal coatings due to the universally adherent nature of phenolic ligands	Difficult to form thin-film coatings without pre-functionalizing the surface of the substrate
	Controllable hydrogel formation	Controllable hydrogel formation
Interaction state	Single or mixed-state dynamic metal chelation	Single-state metal or metal-cluster chelation
	Generally, flexible and tunable coordination networks	Generally, rigid and brittle coordination networks
	Multiplex interactions between MPNs and guests	Weak interactions between MOFs and non-covalently incorporated guests
Porosity	Broad pore size distribution (angstroms to micrometers)	Narrow pore size distribution (angstroms to nanometers) without templating or post-synthesis approaches
	Irregularly interpenetrated pores and channels	Limited regulation over the range of pore sizes arising from the crystal structure (one order of magnitude)

[a] Adapted with permission from ref. 15. Copyright 2023, Springer Nature Limited.

stabilized lysozyme–TA and cytochrome C–TA, but only played minor roles in stabilizing hemoglobin–TA. In contrast, hydrogen bonding and hydrophobic interactions were the main stabilizing forces in immunoglobulin G (IgG)–TA. Generally, an increase in the molecular size of proteins corresponded to stronger hydrogen bonding between TA and the proteins. Additionally, proteins with higher aliphatic indices formed stronger hydrophobic interactions with TA, and proteins with higher isoelectric points typically had stronger ionic interactions with the deprotonated hydroxy moieties of the phenolic groups.

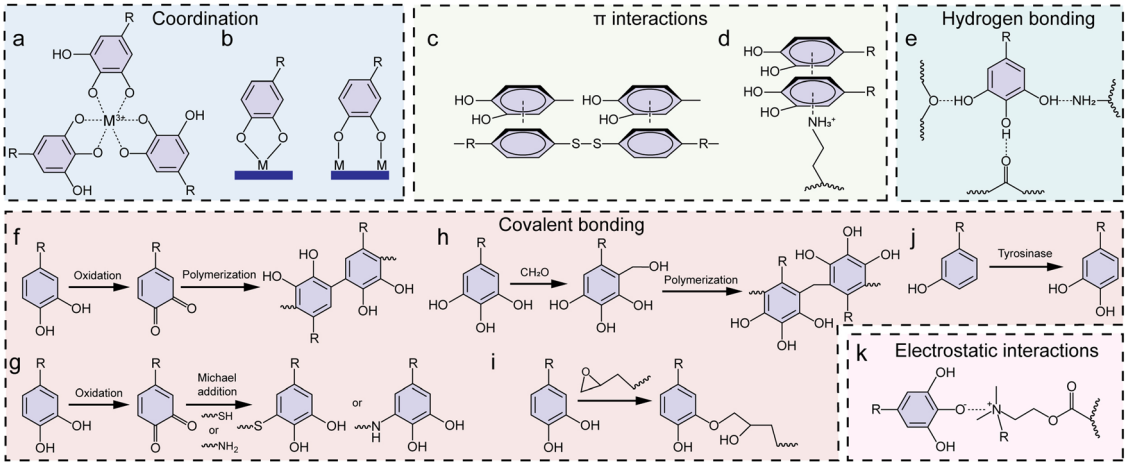

Fig. 5 Polyphenol-mediated interactions of different components in MPN composites.

2.2.3. Customized properties and controllable functionalities for various applications. MPN composites constructed from functional phenolic ligands and metal ions can possess engineered functionalities that are useful for applications spanning the environmental, energy, and biomedical fields. For instance, natural polyphenols are renowned for their diverse biological properties, including antibacterial, anticancer, and neuroprotective effects, rendering them attractive for biomedical applications.[26,49,50] Moreover, the metal-chelating capability of polyphenols enables the integration of multiple metals into the matrix of MPNs, where the properties of the MPN composites, *e.g.*, thickness, stability, pH responsiveness, catalytic activity, and fluorescence, can be tailored through the choice of coordinating metal ions.[24] Importantly, MPNs can simultaneously incorporate metals with widely varying chelation coefficients, thereby facilitating the creation of composite structures that exploit the specific attributes of each metal.[17,24] Tunable metal chelation not only imparts a high degree of customization to the resulting materials but also enables the inclusion of diverse functionalities within a single system.

The dynamic coordination between metal ions and phenolic ligands allows for the disruption and reformation of the coordination bonds in response to various stimuli, such as pH and ionic strength, thereby endowing MPN composites with pH responsiveness, controllable permeability, tunable toughness, and self-healing characteristics (Fig. 6a–c).[51,52] Tunable thickness and kinetic control of MPN composites can also be achieved by engineering the coordination kinetics of phenolic ligands and metal ions (*e.g.*, rust-mediated assembly and oxidation methods).[53,54] For example, the rust-mediated continuous assembly of MPNs involved the use of waste products (*e.g.*, rusty objects) to prepare MPN materials with tailored thicknesses (Fig. 6d).[55] Specifically, a rusted nail (iron(III) oxyhydroxide phases) was immersed in a gallic acid (GA) solution containing polystyrene (PS) particles. The GA solution reacted with the rusted nail and etched the rust layer, generating chelation complexes in solution that self-assembled onto the PS particles to form stable MPN coatings with controllable

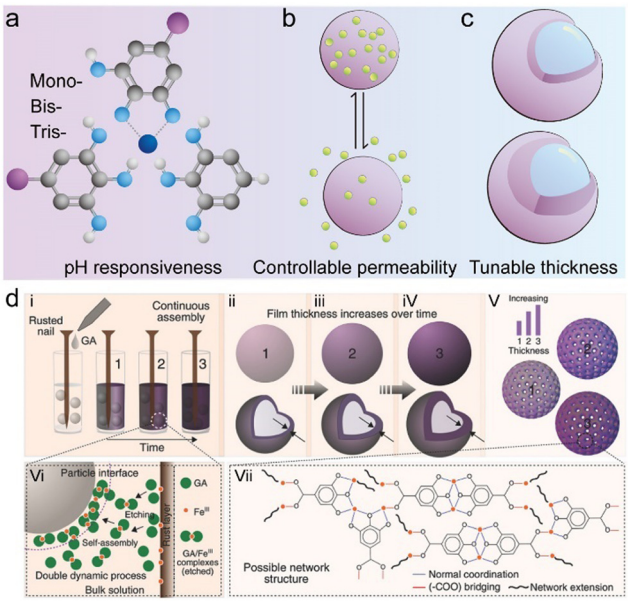

Fig. 6 (a)–(c) Schematic illustration of examples of controllable properties of MPN composites. (d) Schematic illustration of the kinetic control over MPN assembly using rust as a metal source. Adapted with permission from ref. 55. Copyright 2017, Wiley-VCH.

thicknesses from 5 to 70 nm, depending on the immersion time of the rusted nail.

MPN composites can possess desired functionalities (*e.g.*, light responsiveness, glucose responsiveness, and antimicrobial properties) through the selection of precursors for applications across various fields, including catalysis, agriculture, and biomedicine (Fig. 7).[56–59] For example, MPN coatings can enhance the escape of nanoparticles from endosomes—a cellular compartment responsible for internalizing nanomaterials.[60] This offers a simple avenue for achieving the efficient intracellular drug delivery of functional materials. Furthermore, MPN composites (MPN microswimmers), fabricated from ellagic acid and zinc acetate in *N*-methyl-2-pyrrolidone, exhibited tailorable light responsiveness

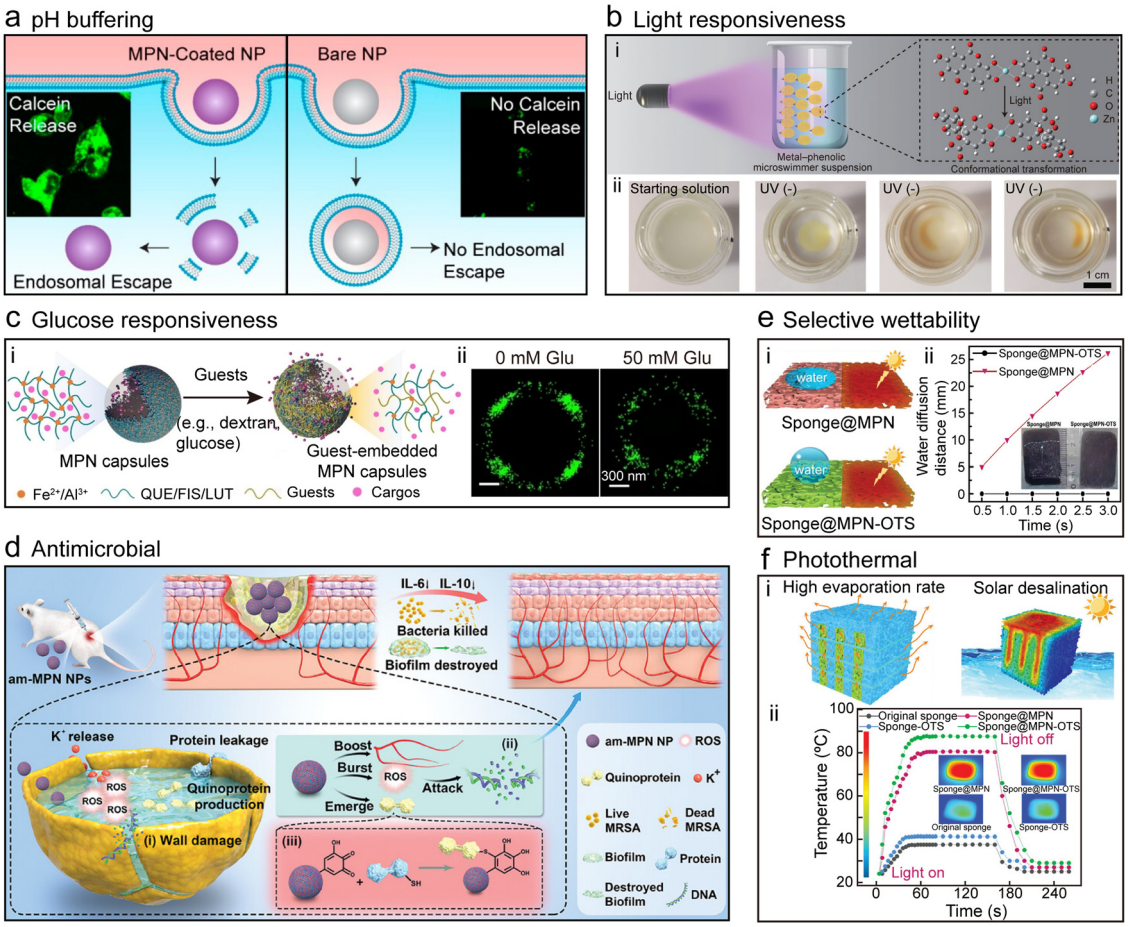

Fig. 7 Properties of MPN composites. (a) pH Buffering, Reproduced with permission from ref. 60. Copyright 2019, American Chemical Society. (b) Light responsiveness, Adapted with permission from ref. 61. Copyright 2021, Wiley-VCH. (c) Glucose responsiveness; QUE, quercetin, Adapted with permission from ref. 52. Copyright 2023, Xu *et al.*, published by Wiley-VCH GmbH. (d) Antimicrobial, Reproduced with permission from ref. 56. Copyright 2023, Yu *et al.*, published by Wiley-VCH GmbH. (e) Selective wettability and (f) photothermal capability, Adapted with permission from ref. 62. Copyright 2022, Wang *et al.*, published by Wiley-VCH GmbH.

(Fig. 7b).[61] Under exposure to UV light (365 nm), ellagic acid underwent structural transformation, leading to an excited state configuration where a single proton transferred from an adjacent hydroxy group to the ether oxygen. The intermediate structure offered a nonradiative structural relaxation pathway, wherein a second proton transfer was coupled with a twist ($\approx$ 55°) in the structure, leading to the formation of a short-lived diketene and a subsequent rapid and reversible twist. The dark region (farthest from the light source) of the MPN microswimmers was more prone to complete relaxation, resulting in more pronounced propulsion alterations to move toward the UV light. In addition, these MPN microswimmers were loaded with functional guests, such doxorubicin (DOX), allowing for the construction of MPN composites with photo-responsive drug delivery properties.

The glucose responsiveness of MPNs was achieved through the comparable binding affinity between glucose and Fe^{2+}, similar to that between quercetin and Fe^{2+} (Fig. 7c).[52] This similarity promoted the incorporation of glucose into MPNs, which induced changes in their physicochemical properties. Consequently, MPN composites loaded with therapeutic agents (*e.g.*, insulin) released the encapsulated cargo in response to fluctuations in glucose concentration. Glucose response was also engineered *via* the use of phenyldiboronic acid molecules that are responsive to glucose.[63]

The antibacterial efficacy of MPN composites originates from the inherent antibacterial properties of the building blocks.[64] For example, antioxidant epigallocatechin gallate (EGCG), Cu^{2+}, and antibacterial diethyldithiocarbamate (DEDTC) were assembled into MPN–DEDTC composites within a few seconds at room temperature, and the composites exhibited potent antibacterial activity against antibiotic-resistant bacteria such as methicillin-resistant *Staphylococcus aureus* (MRSA, Fig. 7d).[56] The MPN–DEDTC composites effectively inhibited bacterial biofilm formation, disrupted existing biofilms, and promoted wound healing in mice infected with MRSA. Systematic investigations revealed that the antimicrobial mechanisms of action of the MPN–DEDTC composites included the formation of quinoproteins, representing a distinct antimicrobial pathway of polyphenol-based MPN–DEDTC composites. Alternatively, Ag^{+} was incorporated into MPNs and deposited onto a variety of substrates to form MPN composites

that neutralized lipid-enveloped viruses, Gram-positive and Gram-negative bacteria, and fungi.[65,66] Importantly, the highly adherent nature of polyphenols afforded a robust antimicrobial coating that could not be removed by soap and water washing.[65] This coating technology was commercialized as the first antimicrobial MPN product to reach the market.

MPNs also exhibit photothermal properties and selective wettability, which are both essential for solar seawater desalination.[67,68] For example, a sponge was incubated with TA and (3-aminopropyl)triethoxysilane (APTES), and Fe^{3+} were then added to cross-link the TA–APTES complexes and form MPN–sponge composites (Fig. 7e and f).[62] The abundant hydrophilic groups of TA rendered the MPN–sponge composites superhydrophilic, whereas the introduction of APTES partially cross-linked the polyphenols, enhancing the stability of the composites. The MPN–sponge composites were further modified with octadecyltrimethoxysilane to form superhydrophobic sponges. Both the modified and unmodified MPN–sponge composites displayed photothermal performance (*i.e.*, temperature increased from 37 °C to 80 °C within 1 min), attributed to the high photothermal conversion efficiency originating from the dark color of Fe^{3+}–TA MPN complexes.

3. Synthesis strategies to engineer MPN composites

The distinct physiochemical properties of MPNs have driven the rapid development of various MPN composites for a wide range of applications. This section will summarize diverse assembly techniques and three strategies that can be employed to synthesize MPN composites, *i.e.*, complexation, template coating, and postmodification, with representative examples highlighted throughout.

3.1. Diverse assembly techniques

The mild synthesis conditions enable the engineering of MPN composites *via* diverse assembly technologies, including immersive assembly, spray assembly, electrotriggered assembly, fluidic assembly, spin assembly, and mechanochemical assembly (Fig. 8). These assembly methods play an essential role in modulating the composition, morphologies, and physicochemical properties of the resulting MPN composites. Therefore, it is important to select the appropriate assembly method for the desired performance, functionality, or application (Table 2).

Immersive assembly is the most common and readily available MPN assembly technique, where generally a functional component (*i.e.*, guest) is transferred to a solvent (*e.g.*, water), and then metal ions or phenolic ligands are added in sequence, followed by optional pH adjustment, leading to the rapid assembly of MPN composites (Fig. 8a).[69–71] Immersive assembly relies on the amorphous characteristics of MPNs, rapid interaction kinetics between metal ions and phenolic ligands, and favorable interactions between ligands and guests.

Spray assembly involves the preparation of metal ions and phenolic ligand solutions that are subsequently nebulized into droplets through a spraying device and deposited onto a functional component (Fig. 8b).[72] This can be done by spraying two solutions alternatively or simultaneously. The solvent on

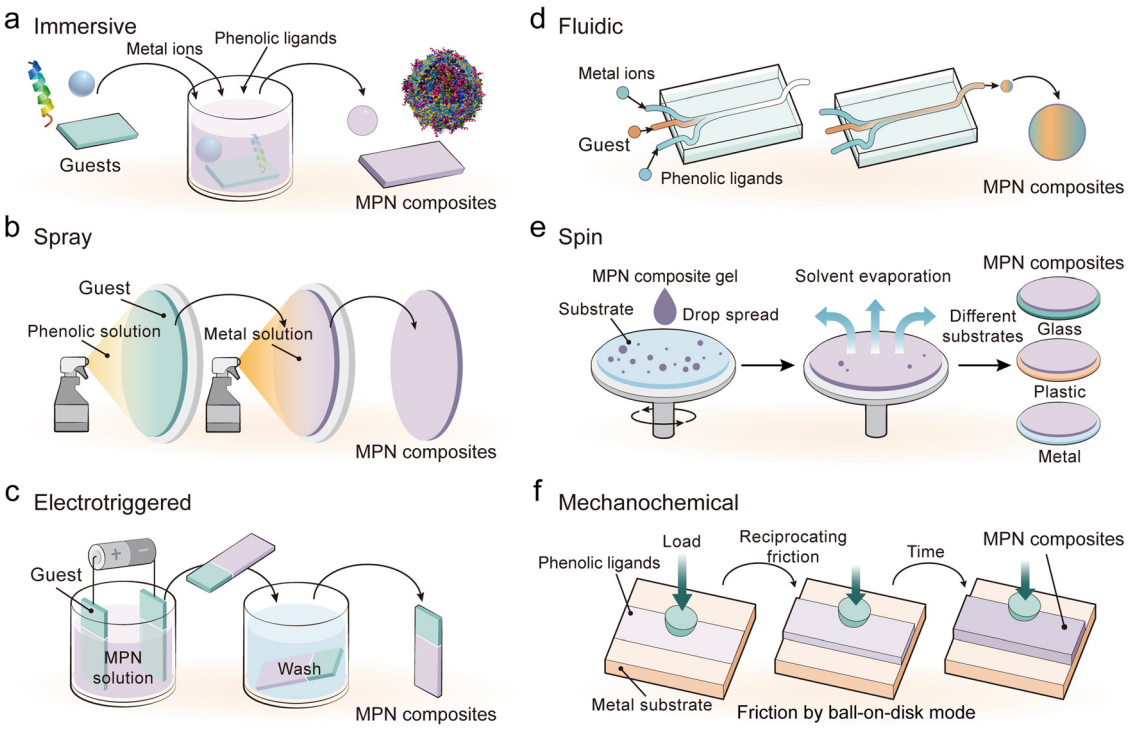

Fig. 8 Schematic illustration of the diverse assembly routes for MPN composites.

Table 2 Comparison of the advantages and disadvantages of different assembly techniques for fabricating MPN composites, and typical applications of resulting MPN composites

Assembly technique	Advantages	Disadvantages	Applications
Immersive	Simple and rapid; accessible for a wide range of substrates; no specialized equipment required	Limited film thickness (~10 nm per deposition cycle); limited control over kinetics and film uniformity; relatively low product yield	Drug delivery and cell targeting;[69] cancer theranostics;[70] bioimaging[71]
Spray	Small (reaction) medium volume; adjustable film thickness; high product yield	Rough film surface; control over spray parameters requires specialized equipment	Antimicrobial coatings;[72] oil–water separation[73]
Electrotriggered	Continuous process; easy separation of MPN composite films; fine-tuning of coating kinetics and thickness	Specialized equipment required; limited to certain metal species; restricted to conductive substrates	Antioxidant coatings;[74] cytocompatible freestanding membranes[75]
Fluidic	Tunable formulation; continuous production capability; controllable particle size	Complex setup with a risk of clogging; precise flow control required	Cell protection;[76] functional nanoparticle formulation;[77] cancer theranostics[78]
Spin	High control over surface and film properties (*e.g.*, uniformity and thickness)	Limited to planar substrates; limited size of substrates	Bone repair;[79] Antimicrobial coatings[80]
Mechanochemical	Solvent-free process; tunable film thickness; large-scale production potential	Specialized equipment required; high energy consumption	Controlled-release fertilizers;[81] functional coatings;[82] catalysts[83]

the surface of the functional component gradually evaporates and subsequently triggers the assembly of MPNs on the functional component. The thickness and uniformity of MPN composites in the spray assembly can be controlled by adjusting the spray parameters (*e.g.*, droplet size, velocity of the spraying solution, order in which solutions are sprayed, and spray angle), solvent type (*e.g.*, water, methanol, and ethanol), precursor concentration, and/or the molar ratio of ligand to metal.[73]

Electrotriggered assembly exploits the inherent charge and redox properties of metal ions and phenolic ligands to rapidly form MPNs.[74] The electric current can significantly accelerate the growth of continuous films by 10–350 times under cytocompatible conditions (*e.g.*, aqueous solution and ambient temperature), and the resulting MPN film can be detached by reversing the potentials of the electrodes.[75] Typically, the guest is submerged into a solution containing metal ions and phenolic ligands and an electric current is applied to move the MPN building blocks toward a substrate with the opposite charge (Fig. 8c). Upon reaching the surface, these charged species undergo chemical interactions, leading to the formation of MPN composites.

Fluidic assembly relies on the manipulation of fluid dynamics within microfluidic channels or regulated flow systems. Generally, solutions containing metal ions, phenolic compounds, and functional components are mixed *via* customizable microfluidic chips with a specific arrangement to control mixing (Fig. 8d).[76–78] The flow rate and order in which solutions are mixed can be adjusted to tune the interaction of the components for the continuous production of MPN composites.

Spin assembly uses high rotational speeds and centrifugal force to evenly spread precursor solutions and evaporate the solvent to form MPN composites (Fig. 8e).[79] The assembly process can be engineered by precursor concentration, coating deposition cycle, solvent type, and spin speed. For example, multiple spin coating processes of MPNs and gallium nanoparticles could generate composites with controllable thickness for tunable Ga^{3+} release behavior.[80]

Mechanochemical assembly is typically a solvent-free process that deprotonates phenolic ligands through friction and subsequently coordinates the deprotonated phenolic ligands with metal ions or oxide to form composites (Fig. 8f).[81–83] For example, composite fertilizers were synthesized through a one-step mixing of phenolic ligands, metal ions, and water-soluble urea, followed by aging or thermal treatment.[81] The integration of MPNs enabled the preparation of urea fertilizers with tunable mechanical resistance, crystallinity (~16%–68%), stiffness (0.1–5.1 MPa), and wettability properties and prolonged urea release profiles (up to 9 days), which are essential for industrial applications.

3.2. Synthesis strategies

3.2.1. Complexation. The fast coordination kinetics between phenolic ligands and metal ions presents both advantages and disadvantages. It facilitates the rapid formation of MPN composites within seconds but it can impede the formation of well-defined nanoparticles.[69,84] Consequently, various seeding agents and/or templates have been employed to modulate the formation of MPN composites during direct complexation. These seeding agents, including small molecules, polymers (*e.g.*, polyvinylpyrrolidone), and biomolecules (*e.g.*, chitosan, proteins), serve to locally increase the concentration of the precursor/s, which consequently accelerates the formation of MPN complexes, even at lower precursor concentrations that are typically less favorable for the formation of MPNs.[85,86] Importantly, these seeding agents (functional components) not only expedite the complexation process but also contribute to stabilizing the resulting composites (Fig. 9a).[87] However, incorporating seeding agents may modify the properties of the nanoparticles (*e.g.*, pH responsiveness).[69] A seeding agent-free strategy was therefore recently developed using specific buffers to mediate the coordination kinetics for directly assembling MPN nanoparticles.[69] A wide range of functional

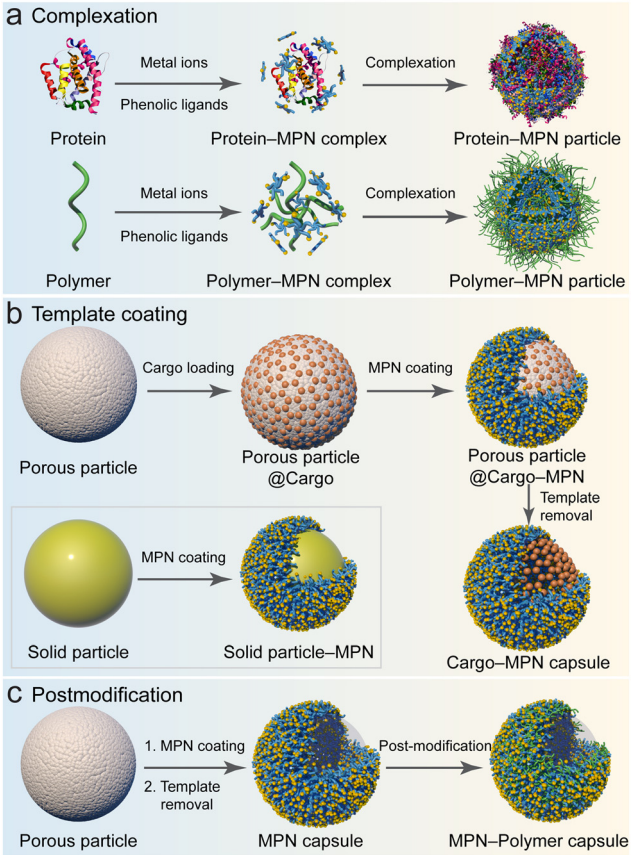

Fig. 9 Strategies for fabricating MPN composites: (a) complexation; (b) template coating; and (c) postmodification. (a) and (c) Adapted with permission from ref. 15. Copyright 2023, Springer Nature Limited.

components, including anticancer drugs and proteins with diverse molecular weights and isoelectric points (*e.g.*, horseradish peroxidase (HRP)), were readily incorporated into these nanoparticles to form composites (Fig. 10a).

The physicochemical characteristics of MPN composite particles can be precisely modulated by manipulating the assembly conditions (*e.g.*, type and concentration of building blocks). For example, a coordination-driven flash nano-complexation process was developed, which employed a turbulent mixing device to achieve the continuous fabrication of quaternary MPNs complexes (Fe^{3+}–TA), HA, and DOX (Fig. 10b).[78] By varying the flow rates of the precursor solutions during mixing, complexes with different sizes were achieved. The size of the complexes was further modulated by adjusting the concentrations of each constituent, as the formation of these complexes was primarily governed by coordination bonds and hydrophobic interactions, which were also pivotal in determining the stability of the resulting nanocomplexes.

Metal–phenolic complexation also allows for the fabrication of bulk composite materials (*e.g.*, supramolecular gels).[88] For example, high ratios of Ti^{4+} to TA (*e.g.*, 5 : 1) in *N*,*N*-dimethylformamide or water facilitated the direct formation of MPN gels that could be used as matrixes for active pharmaceutical ingredient crystallization.[89] These MPN–drug

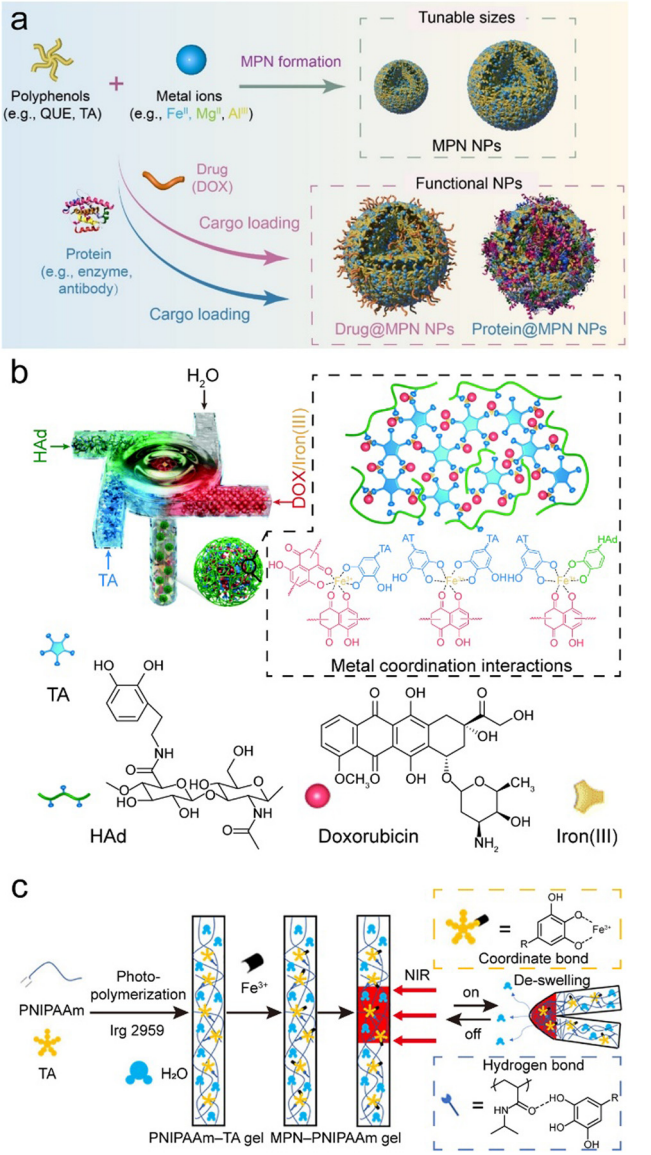

Fig. 10 (a) Complexation method for forming MPN composites. NPs, nanoparticles. Reproduced with permission from ref. 69. Copyright 2023, Xu *et al.*, published by Wiley-VCH GmbH. (b) Coordination-driven rapid complexation of MPN–dopamine-modified hyaluronic acid (HAd)–DOX nanoparticle composites using a turbulent mixing device. Reproduced with permission from ref. 78. Copyright 2019, Royal Society of Chemistry. (c) Synthesis and NIR-triggered actuation (reversible bending–unbending) of MPN–PNIPAAm composite hydrogels. Adapted with permission from ref. 42. Copyright 2021, American Chemical Society.

composites allow for the continuous release of drugs, highlighting significant potential as drug delivery systems.[90] MPN composite gels also display temperature- and pH-sensitive properties *via* direct assembly. For example, MPNs made of Fe^{3+}–TA could act as a photothermal transmitter and combined with poly(*N*-isopropylacrylamide) (PNIPAAm) to form smart hydrogels, where TA formed hydrogen bonds with PNIPAAm during *in situ* polymerization (Fig. 10c).[42] The inclusion of MPNs improved the mechanical properties of PNIPAAm hydrogels, and the MPN–PNIPAAm composite hydrogel exhibited

photothermal properties and reversible deformation behaviors under near-infrared (NIR) irradiation. Similarly, responsive hydrogels, *i.e.*, MPN–aminoglycoside composites, demonstrated dynamic characteristics and responded to various stimuli (temperature, light, pH, electricity, and redox) and displayed antibacterial activity.[91] In general, MPN composite hydrogels hold promise for a variety of biomedical applications, for example, as wound dressings (antioxidant and provascularization activity) and as bioadhesives.[92–94]

3.2.2. Template coating. MPN coatings can be assembled on a broad range of substrates, including organic, inorganic, and biological entities (Fig. 11a). Directly assembling MPNs on functional templates (*e.g.*, drug or Fe_2O_3 particles,) leads to core–shell composites (Fig. 9b), where the MPNs act as protective barriers for the cores and thereby increase the stability of the composite.[95] For example, most anticancer drugs (*e.g.*, paclitaxel) are hydrophobic and typically suffer from low solubility in aqueous environments, resulting in low bioavailability and unfavorable pharmacokinetics.[96] Owing to the aromatic structure of phenolics, MPNs can be deposited on hydrophobic drug particles *via* hydrophobic interactions and π–π interactions (Fig. 11b), where the negatively charged catechol and gallol moieties prevent the drug particles from aggregation by increasing the interparticle electrostatic repulsion.[95,97–100] MPN coatings also facilitate the formation of small, uniform, and stable drug composites, which are useful for enhancing the antitumor activity of drugs both *in vivo* and *in vitro*.[95] Furthermore, MPNs can prevent the aggregation of inorganic nanoparticles (*e.g.*, gold nanoparticles) and enhance their catalytic activity *via* synergistic effects.[101]

MPN coatings are also widely exploited as a gating layer on porous substrates (*e.g.*, mesoporous silica) for controlled release (Fig. 9b).[103–105] For example, porous substrates were incubated with functional components (*e.g.*, drugs) at a high loading capacity, and the surface of the substrates was then coated with MPNs to prevent burst release.[104] Drug-loaded MPN capsules were obtained after selective removal of the templates (*e.g.*, using ethylenediaminetetraacetic acid to remove $CaCO_3$ templates).[106] These MPN composite capsules were pH responsive and were used for intracellular cargo release owing to the disassembly ability of MPNs in acidic environments, *i.e.*, endosomal/lysosomal compartments (Fig. 11c).[102,107,108]

3.2.3. Postmodification. The surface properties (*e.g.*, charge) of nanomaterials play an essential role in governing their interactions with other materials and the external environment.[109,110] Therefore, modifying the surface of materials with specific chemical moieties (*e.g.*, targeting or low fouling) is important for achieving specific functions, particularly for biomedical applications.[111] The amorphous and supramolecular nature of MPNs allows for the MPN coatings to be easily modified by diverse functional materials (*e.g.*, polymers, protein corona) to increase their stability or endow them with certain properties (Fig. 9c). For example, the direct deposition of a protein corona from human serum on MPN–HA composite

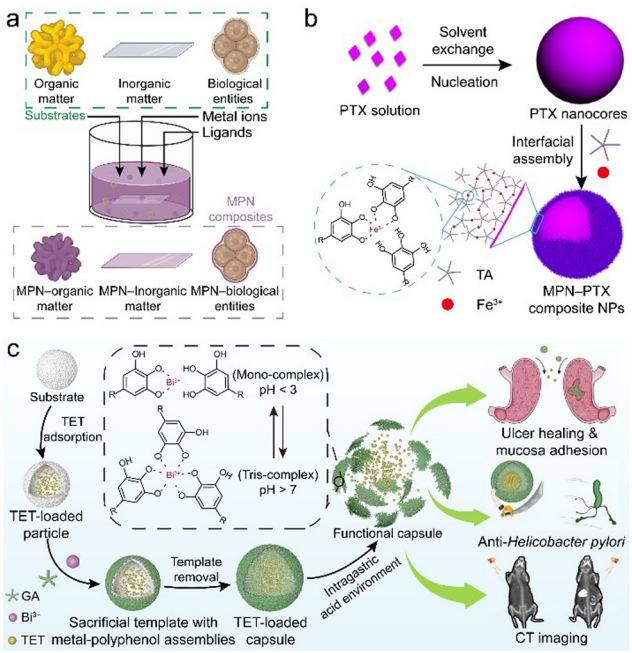

Fig. 11 (a) MPN coating on different templates (*e.g.*, organic, inorganic, and biological entities). (b) Synthesis of MPN–paclitaxel composite nanoparticles. PTX, paclitaxel. Adapted with permission from ref. 95. Copyright 2016, American Chemical Society. (c) Synthesis and therapeutic applications (*e.g.*, ulcer healing, anti-*Helicobacter pylori*, and computed tomography (CT) imaging) of MPN–tetracycline composite capsules. *TET*, tetracycline. Adapted with permission from ref. 102. Copyright 2022, Wiley-VCH.

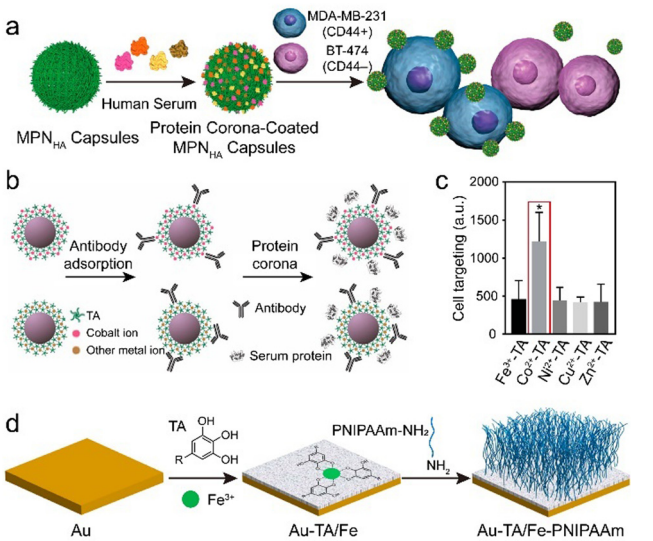

Fig. 12 (a) Synthesis of MPN–HA composites with customized protein coronas *via* postmodification of MPNs. Adapted with permission from ref. 112. Copyright 2016, American Chemical Society. (b) Synthesis of MPN–gold nanoparticle–antibody composites *via* postmodification. (c) Cell targeting of different MPN–gold nanoparticle–antibody–protein corona composites to BT-474 (Her2+) cells. (b) and (c) Adapted with permission from ref. 113. Copyright 2020, American Chemical Society. (d) Synthesis of gold (Au)–TA/Fe–PNIPAAm surfaces. Adapted with permission from ref. 114. Copyright 2020, American Chemical Society.

capsules increased their targeting specificity by reducing nonspecific cell interactions (Fig. 12a).[112] The presence of the protein corona reduced the exposure of the highly adherent phenolic groups to cells, and their nonspecific interactions were reduced to 9% compared to the MPN–HA composite (prepared from a low molecular weight HA) without a protein corona (*e.g.*, 47%), while their cancer cell targeting was maintained, resulting in a three-fold improvement in cell selectivity. Furthermore, the metal ions in MPNs, particularly Co^{2+}, facilitated the orientation of antibodies on their surfaces, enabling high antibody–antigen recognition (Fig. 12b and c).[113]

The MPN surface can also be covalently modified by polymers through reaction of the phenolic hydroxy group of the polyphenols with amine-terminated polymers *via* Michael addition or Schiff base reactions. For example, an antibacterial film was constructed based on MPNs and the subsequent attachment of a temperature-responsive PNIPAAm film *via* a "grafting-to" method (Fig. 12d).[114] The MPN composites resulted in a reduction of >99% in bacteria owing to the photothermal effects of the Fe^{3+}–TA complexes under NIR irradiation, and this bactericidal efficiency was further enhanced by the thermally activated repellent properties of PNIPAAm.

4. Design of functional MPN composites and applications

The composition of MPN composites dictates their physicochemical properties and intended applications. This section discusses various MPN composites based on different functional components, including small molecules, polymers, biomacromolecules, metal nanoparticles, oxides, and biological entities. We highlight the synergistic effects of MPNs and the functional components to demonstrate the advantages of MPN composites and to provide a guideline for the rational design of MPN composites tailored for specific applications.

4.1. MPN-small molecule composites

Small molecules, including organic dyes, fluorescent probes, therapeutic drugs, antibacterial agents, and molecular imaging agents, have been used to form functional MPN composites.[115,116] The obtained MPN composites can enhance the bioactivity of therapeutic small molecule drugs in multiple aspects, including extending circulation time, controlling release, and improving targeting.

MPNs provide a platform for the incorporation of aromatic dyes and can therefore be used to devise versatile fluorescence labeling strategies.[115,117] For example, fluorescence properties were incorporated into substrates (*e.g.*, PS, SiO_2, gold nanoparticles, resin, melamine formaldehyde, and *Escherichia coli*) by directly mixing TA, metal ions (*e.g.*, Zr^{4+}, Fe^{3+}, Al^{3+}), and fluorescent dyes (rhodamine B, rhodamine 6G, and perylene) to form MPN–dye composites *via* supramolecular interactions (Fig. 13a–c). This approach circumvents the use of expensive imaging probes or complex covalent conjugation. The engineered luminescent MPN composites were used as tracers for the visualization of intracellular interactions, drug delivery, and biodistribution studies (Fig. 13d and e).

Small molecules can also be incorporated inside MPNs *via* Schiff base cross-linking or Michael addition between catechol groups and thiols or amines.[51,119] For example, the amino group of selenocystamine (SeCA) demonstrated reactivity with the gallic group of GA, and MPN composites composed of Cu^{2+}–GA MPNs and SeCA were developed as functional coatings for generating therapeutic nitric oxide (NO) (Fig. 13f).[118] The production rate of NO was adjusted over a wide range by controlling the amount of Cu^{2+} in the coatings, with a 5-fold higher production than that achieved by GA/SeCA alone owing to the synergism of the two metals in a single system (Fig. 13g and h). The NO-generating coatings effectively inhibited platelet activation and smooth muscle cell proliferation and supported endothelial cell growth for treating cardiovascular disease. These features are essential for inhibiting thrombogenicity and restenosis and enhancing reendothelialization from implanted biomedical devices (*e.g.*, cardiovascular stents).

Conventional disease treatments using small molecules commonly suffer from off-target effects that can cause side effects, including drug resistance, shorter blood circulation, and damage to normal tissue.[120,121] The immobilization of drugs in MPNs to form MPN–drug composites is a promising approach for solving these issues. For example, the anticancer drug DOX was loaded into MPNs to form therapeutic nanoparticles *via* coordination bonds and π–π interactions between DOX and the MPNs.[122] The MPN–DOX composites exhibited multiple therapeutic properties, including photothermal effects, ferroptosis, and chemotherapeutic effects. Specifically, the temperature of the solution containing the MPN–DOX composites increased up to approximately 60 °C following 10 min of irradiation owing to the ligand-to-metal charge-transfer band. The MPN–DOX composites also produced ROS, facilitating both ferroptosis and the deep penetration of DOX into tumors. The chemotherapeutic effects of DOX enhanced the ferroptosis efficiency by oxidation–reduction cascade reactions, and the composites maintained a high tumor inhibition ratio using low doses of DOX and Fe^{3+}. Other small molecular drugs (*e.g.*, bortezomib, romidepsin, and venetoclax) were also incorporated into MPNs for diverse potential applications, including cell apoptosis, reactivation, and biomedical imaging (Fig. 13i–k).[116] Moreover, owing to the modularity of the assembly process, the functionality of the MPN-composites can be expanded by incorporating targeting ligands post assembly and sequentially assembling additional small molecules, advancing MPN-composites for nanomedicine and biotechnology.

4.2. MPN–polymer composites

Polymers typically possess lightweight properties, high processibility, and high thermal and chemical stability. The low cost and versatile chemistry of polymers enable the preparation and usage of MPN composites in the form of hydrogels, membranes, and other macroscopic materials for industrial and

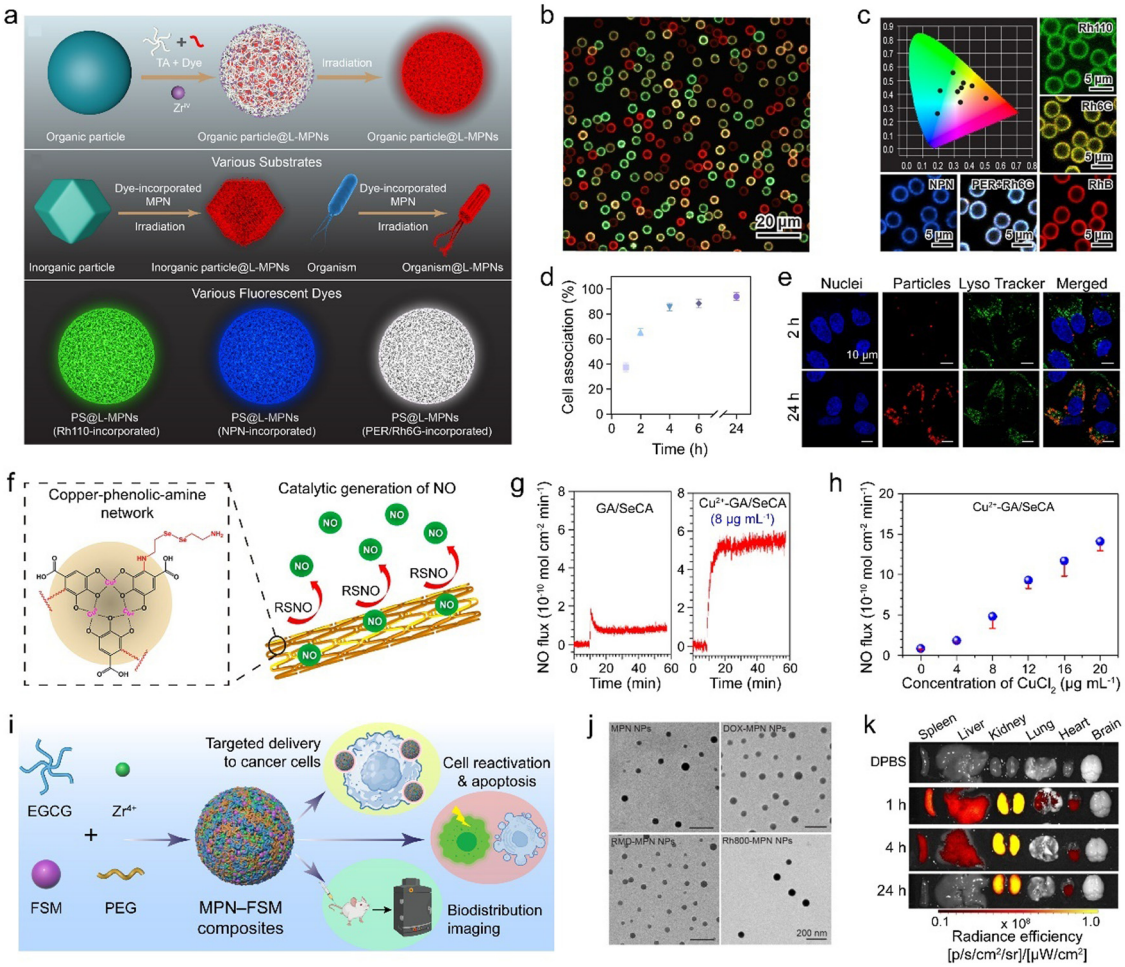

Fig. 13 (a) Synthesis of luminescent MPN–dye composites with different functional components and different dyes to achieve tunable light emission. (b) Confocal laser scanning microscopy (CLSM) image of MPN–dye composites with a variety of emission colors. (c) CIE chromaticity coordinates of different luminescent MPN–dye composites. Rh110, rhodamine 110 chloride; Rh6G, rhodamine 6G; PER, perylene; RhB, rhodamine B. (d) Association of MPN–dye composites with HeLa cells at 37 °C over time. (e) CLSM images of MPN–dye composites in HeLa cells. (a)–(e) Adapted with permission from ref. 115. Copyright 2021, Wiley-VCH. (f) MPN–SeCA composites can produce therapeutic NO for treating cardiovascular disease. (g) Comparison of NO generation between GA/SeCA and MPN–SeCA composites and (h) effect of the concentration of chelated Cu^{2+} on NO generation. (f)–(h) Adapted with permission from ref. 118. Copyright 2018, American Chemical Society. (i) Synthesis and application of MPN–functional small molecule (FSM) composites. (j) Transmission electron microscopy (TEM) images of MPN and MPN–FSM composite nanoparticles. The FSMs include DOX, rhodamine 800 (Rh800), and romidepsin (RMD). (k) Biodistribution of MPN–FSM (Rh800) composites in major organs. (i)–(k) Adapted with permission from ref. 116. Copyright 2024, Chen *et al.*, published by Wiley-VCH GmbH.

biomedical applications.[86,123] For example, ultrasmall nanodots (*i.e.*, MPN–polyvinylpyrrolidone (PVP) composites) were synthesized at the gram scale *via* the coordination of Fe^{3+}, GA, and PVP in ambient conditions (Fig. 14a).[85] Each component was essential for forming the nanodots, as low-quality particles with irregular shapes were observed when only two of the three components were used. PVP acted as a protective polymer during the nucleation and growth of the MPN composite nanodots because the amide moieties of PVP can coordinate with Fe^{3+}, thus sterically stabilizing the nanodots. The surface of the nanodots was covered by the neutral PVP layer rather than the negatively charged MPN layers, thereby reducing the adsorption of proteins (Fig. 14b and c). The acidic environment of the tumor region activated magnetic resonance imaging (MRI) contrast owing to the enhanced quantity and mobility of coordination water surrounding the Fe paramagnetic center caused by the reduced coordination state of the chelation complexes. The composite nanodots displayed photothermal performance for suppressing tumor growth. Importantly, the nanodots accumulated in tumor sites *via* the enhanced permeability and retention effect and were subsequently rapidly excreted *via* renal clearance (Fig. 14d and e).

Directly mixing polymers, phenolic ligands, and metal ions presents a simple approach to assemble MPN composites, but MPN composites can also be obtained by conjugating the phenolic ligands to polymers, and then using the phenolic-carrying polymers to chelate metal ions and functional components to form MPN composites.[128] For example, caffeic acid (CAF), a phenolic compound characterized by a carboxylic acid moiety, was conjugated to an amine-functionalized PEG

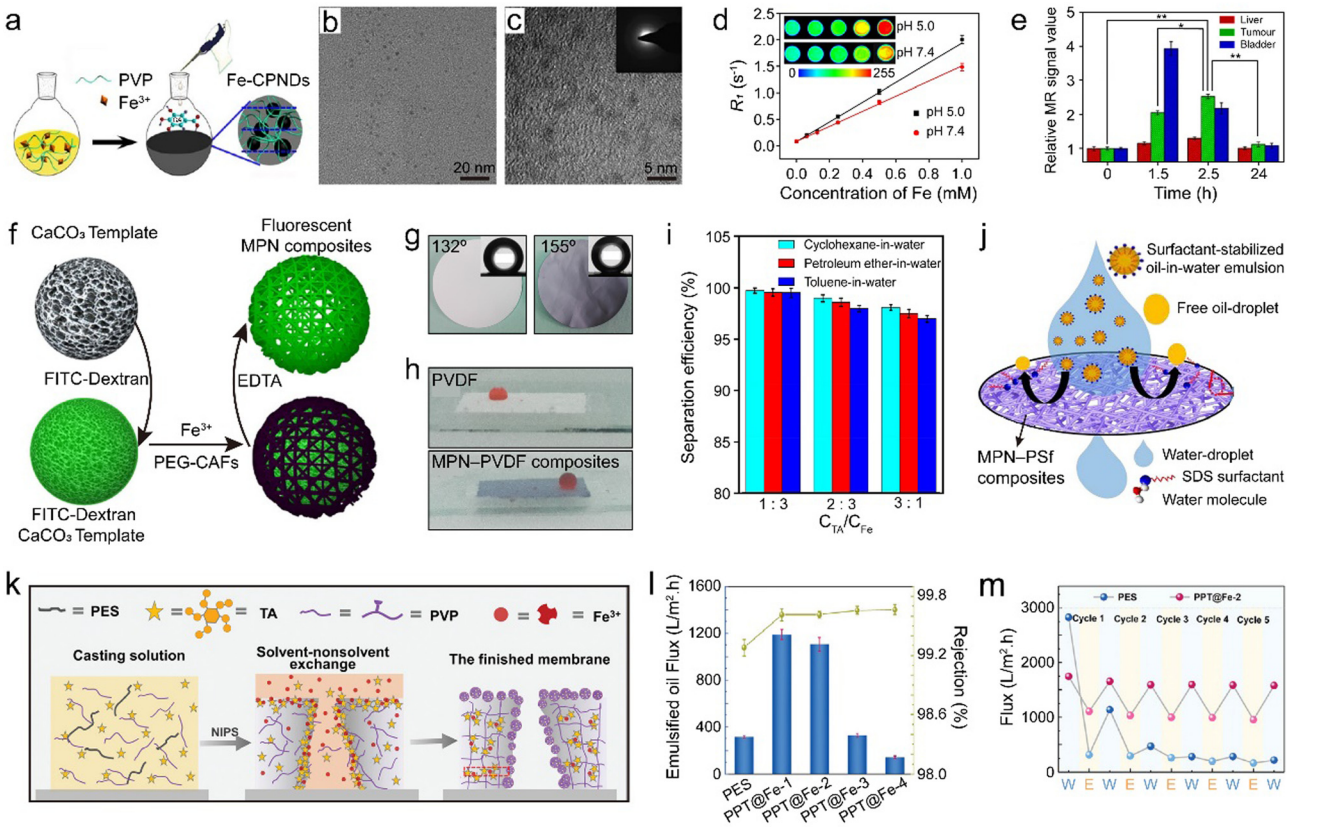

Fig. 14 (a) Synthesis of MPN–PVP composites. CPNDs, coordination polymer nanodots. (b) TEM and (c) high-resolution TEM images of MPN–PVP composites. (d) R1 relaxivity of MPN–PVP composites as a function of Fe^{3+} concentration at different pH values. Inset: Corresponding MRI images of MPN–PVP composites at different pH values. (e) Relative MR signal value of tumor and main organs over time. (a)–(e) Adapted with permission from ref. 85. Copyright 2015, Liu *et al.* (f) Synthesis of fluorescent MPN composites using PEG–CAFs. Adapted with permission from ref. 124. Copyright 2021, American Chemical Society. (g) Underwater oil contact angles and (h) photographs of underwater oil droplets on the surfaces of pure PVDF and MPN–PVDF composite membranes. (i) Effect of the TA and Fe^{3+} concentration ratio on the separation performance of MPN–PVDF composite membrane. (g)–(i) Adapted with permission from ref. 125. Copyright 2020, Elsevier B.V. (j) Schematic of the emulsion separation mechanism of MPN–PSf composites. Adapted with permission from ref. 126. Copyright 2021, Elsevier B.V. (k) Schematic of the formation mechanism and (l) flux of oil-in-water emulsions and rejection rate of MPN–PES/PVP composite ultrafiltration membranes. PPT refers to PES/PVP/TA. (m) Water flux (W) and emulsified oil flux (E) of PES and MPN–PVP/PES composite ultrafiltration membranes over five cycles. (k)–(m) Adapted with permission from ref. 127. Copyright 2022, Wiley-VCH GmbH.

polymer *via* amide formation, resulting in the formation of polymerized caffeic amide (PEG–CAFs).[124] This method offers a convenient alternative for synthesizing customized PEG-based phenolic macromolecules and shows potential utility in the fabrication of MPN composite capsules. For example, fluorescent MPN composite capsules were synthesized using PEG–CAFs, Fe^{3+}, and fluorescein isothiocyanate (FITC)–dextran *via* templating, with potential for the delivery of drugs or therapeutic nucleic acids (Fig. 14f). Furthermore, MPN–PNIPAAm composite capsules were prepared using Fe^{3+} and α,ω-biscatechol-functionalized PNIPAAm (biscatechol–PNIPAAm). Biscatechol–PNIPAAm was synthesized by reversible addition–fragmentation chain transfer polymerization using a symmetrical trithiocarbonate chain transfer agent with two catechol groups.[34] Owing to the incorporation of PNIPAAm chains into the capsule shell, the MPN–PNIPAAm composite capsules demonstrated reversible thermoresponsive properties. Upon exceeding the lower critical solution temperature (LCST), PNIPAAm underwent a conformational transition from water-swollen to dehydrated, leading to a reduction in the size of the MPN–PNIPAAm composite capsules, concurrent with an increase in shell thickness and a decrease in permeability. This temperature-dependent permeability was modulated to enable dynamic encapsulation and release of cargo. For instance, at 25 °C, 500 kDa FITC–dextran readily permeated the capsules. In contrast, upon elevation of the temperature beyond the LCST, FITC–dextran became encapsulated within the capsules as the shell became impermeable. Subsequent reduction of the temperature below the LCST prompted the release of the encapsulated FITC–dextran as the shell returned to a permeable state. Such MPN–PNIPAAm composite capsules hold promise for applications in vaccination and pulmonary delivery.

MPNs have been extensively used to modify the surface of polymer membranes, particularly for separation (*e.g.*, oil/water separation, seawater desalination), catalysis (*e.g.*, organic pollutant degradation), and pollutant adsorption (*e.g.*, dyes, heavy metals).[129] Nano-composite membranes of Fe^{3+}–TA@polyvinylidene fluoride (PVDF) (MPN–PVDF composites) with

superhydrophilicity were designed *via* the assembly of Fe^{3+} and TA on PVDF membranes for oil–water separation (Fig. 14g and h).[125] The MPN–PVDF composite membranes exhibited a separation efficiency of up to 99.5% for oil-in-water emulsions owing to the hydrophilicity and roughness of the MPN layer (Fig. 14i).

MPNs are compatible with a variety of assembly technologies such as electrospinning. For example, electrospun MPN nanofiber membrane (*i.e.*, polysulfone, PSf) composites demonstrated superhydrophilicity in air and under oil, coupled with underwater superoleophobicity, which facilitated the separation of oil-in-water mixtures and surfactant-stabilized oil-in-water emulsions, achieving flux values of 6.5×10^4 and $>6.0 \times 10^3$ L m^{-2} h, respectively (Fig. 14j).[126] Moreover, these composites demonstrated a high recovery capacity (99.8%) and a high oil rejection (99.9%).

MPNs can also control surface segregation behaviors during nonsolvent-induced phase separation. For example, an Fe^{3+}-induced phase transformation strategy was employed in a one-step method to prepare polyethersulfone (PES) ultrafiltration membranes featuring an antifouling structure, which generated interfacially assembled MPN–PVP nanospheres in the PES matrix (Fig. 14k).[127] Antifouling properties were attributed to concentration changes caused by distinct surface separation behaviors exhibited by the hydrophilic additives PVP and TA during the nonsolvent-induced phase separation process. The MPN–PVP/PES composite ultrafiltration membranes showed superhydrophilic and underwater superoleophobic performance, and high separation efficiency, achieving a flux surpassing 1100 L m^{-2} h and a rejection rate exceeding 99.5% for oil-in-water emulsion separation (Fig. 14l). Notably, these composites exhibited sustained performance, with the flux recovery rate remaining at 90% after 5 cycles and 86% after 30 cycles (Fig. 14m). Moreover, the porous MPN–PVP/PES composite ultrafiltration membranes displayed self-cleaning properties, suggesting that they meet the requirements for large-scale oil/water separation applications.

4.3. MPN–biomacromolecule composites

Biomacromolecules are large biomolecules typically with molecular weights higher than 1000 Da, such as proteins, many nucleic acids, and various polysaccharides.[130] The biological activity (*e.g.*, enzymatic catalysis) of biomacromolecules is generally high under mild biological conditions but rapidly decreases in harsh conditions (*e.g.*, organic solvents or high temperature). Furthermore, the direct recycling of biomacromolecules is typically complicated and time-consuming owing to their high solubility, propensity to denature, and relatively small size.[131] Incorporating biomacromolecules into MPNs can increase their recyclability and shield the biomacromolecules from denaturing conditions. In contrast to crystalline MOF materials, MPNs afford the easy incorporation of biomacromolecules with different sizes, shapes, and surface charges *via* pre- or post-loading owing to the large pore size distribution and diverse interactions of MPNs.[69] Moreover, the high permeability of MPNs can facilitate the diffusion of reactants through the composites without completely isolating the biomacromolecules.

The assembly of functional MPN–biomacromolecule composite nanoparticles can be readily accomplished in water by mixing polyphenols, metal ions, and biomacromolecules.[69,132] Assembly is primarily driven by the hydrophobic interactions and coordination of metal–phenolic complexes, resulting in the formation of uniform spherical nanoparticles, generally smaller than 200 nm. Moreover, this method retains the functionality of the biomolecules (*e.g.*, HRP and glucose oxidase) and allows their use in various applications, including biocatalysis and cancer therapy. This platform offers a streamlined approach for engineering bioactive MPN composites.

A soft template method was developed to fabricate functional MPN–biomacromolecule composite microcapsules by depositing MPNs (Fe^{3+}–TA) on bovine serum albumin (BSA) microbubbles (Fig. 15a).[133] The application of heat and ultrasound increased the amount of β-sheet structures in BSA, thereby enhancing the overall stability of the BSA–MPN microbubbles. Furthermore, the synergistic interactions of TA and Fe^{3+} increased the percentage of short peptide chains connecting α-helix fragments within BSA, which consequently reduced the shell resistance of the BSA microbubbles, facilitating the release of gas contained within the microbubbles (Fig. 15b–d). Notably, the BSA microbubbles were used as templates for generating other MPN composites (*e.g.*, Cu^{2+}–TA–BSA and Ni^{2+}–TA–BSA) and could transport functional substances (*e.g.*, magnetic nanoparticles, FITC, and tetramethylrhodamine isothiocyanate-dextran), demonstrating promise for drug delivery (Fig. 15e).

The administration of certain peptides for therapeutic purposes is challenged by their short half-life in the body, which necessitates frequent injections to maintain the effective concentration, in turn increasing the possibility for complications.[135] The use of MPNs as protective coatings has emerged as an effective strategy to address this issue. For example, liraglutide (Lira) is a therapeutic peptide with a short half-life (~13 h) that is used for treating Type II diabetes, and frequent injections are required to maintain an effective drug concentration in the blood.[136] The encapsulation of Lira inside MPNs (MPN–Lira composites) offered an effective strategy to extend the release of Lira over 8 days *in vitro* in phosphate-buffered saline.[136] The formation of MPN–Lira composites was driven by hydrogen bonding between TA and Lira, and metal ions were then added to cross-link the drug complexes and control their size. Both free Lira and MPN–Lira composites effectively reduced the blood glucose level (BGL) within the first 6 h. However, the BGL of the mice dosed with free Lira rapidly rebounded in the next 36 h, whereas the BGL of the mice dosed with MPN–Lira composites was effectively maintained for the next 156 h owing to the slow release of Lira from the composite system.

Targeted drug delivery is important for disease treatment. It relies on specific recognition motifs, such as antibody–antigen recognition, to precisely direct drug delivery vehicles to target sites.[137] The metal ions of MPNs can direct the orientation of antibodies on the MPN surface and achieve high antibody–antigen recognition for targeting.[113] For example, the targeting

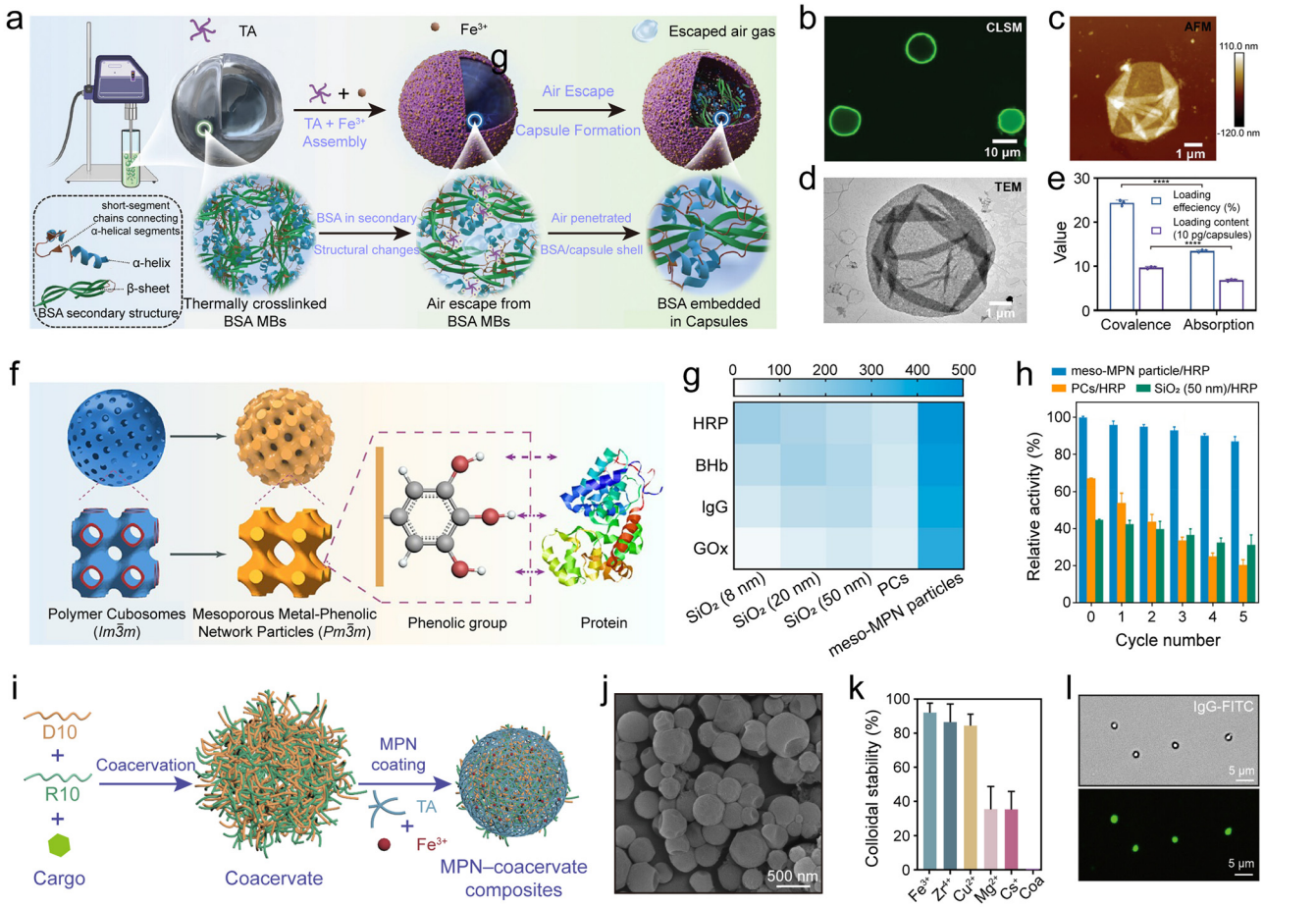

Fig. 15 (a) One-step synthesis of MPN–BSA composites. MBs, microbubbles. (b) CLSM, (c) atomic force microscopy, and (d) TEM images of MPN (Fe^{3+}–TA)–BSA capsules. (e) Loading efficiency and loading content of MPN–BSA composites pre-encapsulating guests *via* covalent binding and physical adsorption. (a)–(e) Adapted with permission from ref. 133. Copyright 2023, Wiley-VCH. (f) Synthesis of mesoporous MPN–protein (*e.g.*, HRP, BHb, IgG, and GOx) composites. (g) Comparison of protein loading of meso-MPN particles and SiO_2 particles. (h) Recyclability of meso-MPN particles. (f)–(h) Adapted with permission from ref. 21. Copyright 2019, American Chemical Society. (i) Formation of MPN–coacervate composites. D10, polyAsp; R10, polyArg. (j) SEM image of MPN–coacervate composites. (k) Colloidal stability of coacervates and MPN–coacervate composites prepared with different metal ions in phosphate buffer. Coa, coacervate. (l) Bright-field (top) and fluorescence microscopy (bottom) images of MPN–coacervate composites loaded with IgG–FITC. (i)–(l) Adapted with permission from ref. 134. Copyright 2023, American Chemical Society.

ability of MPN–antibody composites using Co^{2+} was two times higher than that of other metal-based MPN composites (*e.g.*, Fe^{3+}, Ni^{2+}, Cu^{2+}, and Zn^{2+}). The higher targeting ability was ascribed to the selective orientation of the antibodies on MPNs mediated by the exposed Co^{2+}, rather than any increase in the amount of antibody. The higher concentration of Co^{2+} exposed to solvent (compared with other metals) promoted coordination binding with the histidine-rich fragment crystallizable region of the antibodies, thus effectively anchoring the antibodies to the MPN-coated nanoparticles. The MPN-mediated assembly of oriented antibodies is expected to provide a facile way for modifying diverse particles for targeted drug delivery.

Fibronectin (FN), which contains RGD (Arg–Gly–Asp) polypeptide sequences, is a promising targeting ligand for cancer cells that have a high level of $\alpha_v\beta_3$ integrin expression, and this sequence therefore offers opportunities to achieve targeted drug delivery in cancer therapy.[138] For example, MPN–DOX@FN nanocomposites were prepared by the direct mixing of TA, Fe^{3+}, and DOX to form MPN–DOX composites, which were subsequently coated by FN *via* hydrogen bonding to allow for targeted multimodal tumor therapy, including chemotherapy and immunotherapy.[139] The MPN–DOX@FN composites showed a pH-dependent release for both DOX and iron ions, allowing for synergistic effects between iron-based chemokinetic therapy and DOX chemotherapy to lower the viability of cancer cells. The administration of programmed cell death ligand 1 (PD-L1) antibodies as a component of the immune checkpoint blockade could augment the effectiveness of tumor treatment and trigger a beneficial immune response. The MPN–DOX@FN composites selectively targeted tumor cells that had a high expression of $\alpha_v\beta_3$ integrin, while also demonstrating an r_1 relaxivity of 6.1 mM^{-1} s^{-1} owing to the presence of iron, rendering them suitable for imaging tumors with T_1-weighted MRI. This multimodal delivery and targeting approach offers potential for cancer treatment and diagnosis.

Porous materials hold significant scientific and industrial importance, with those having ordered mesopores exceeding 20 nm in size being particularly promising for applications that involve biomacromolecules and nanoparticles, such as drug delivery.[140] A templating strategy was reported to synthesize ordered mesoporous MPN particles that could load and protect biomolecules (Fig. 15f).[21] Specifically, polystyrene-*block*-poly(ethylene oxide)-assembled polymer cubosomes (PCs; $Im\bar{3}m$) were employed as templates to synthesize mesoporous MPN (meso-MPN) particles, where large-pore ($\sim$40 nm) single networks ($Pm\bar{3}m$) were replicated by the *in situ* formation of MPNs followed by dissolution of the PC templates with tetrahydrofuran. Various meso-MPN particles were designed using a variety of phenols (*e.g.*, EGCG and GA) and metal ions (*e.g.*, Fe^{3+}, Cu^{2+}, and Zr^{4+}) and served as carriers for encapsulating a wide range of biomacromolecules (*e.g.*, HRP, bovine hemoglobin (BHb), IgG, and glucose oxidase (GOx), Fig. 15g). For example, the loading capacity for HRP was 486 mg g^{-1}, which was $\sim$3- and $\sim$5-fold higher than the amounts loaded in the SiO_2 particles with average pore sizes of 8 and 50 nm, respectively. Notably, meso-MPN–HRP composite particles demonstrated high catalytic activity (82% of the free enzyme) and recyclability, with only a decrease of 13% in activity observed over five cycles (Fig. 15h).

Coacervates formed from biomolecules (*e.g.*, peptides, nucleic acids) *via* liquid–liquid phase separation create enclosed compartments that mimic cellular organization and therefore offer a versatile platform for studying cell prototypes and synthetic biology in general.[141] However, membrane-free coacervates are prone to coalesce and suffer from poor structural stability.[142] MPNs are promising platforms for mimicking cell membranes owing to their ability to self-assemble on the surface of coacervates in biological environments and to endow them with desirable properties, including cellular protection, controllable permeability, and physicochemical stability. For example, peptide coacervates emulating the cytoplasm were coated by MPNs as a synthetic cell membrane.[134] Specifically, polyarginine (R10) and polyaspartic acid (D10) formed coacervates through liquid–liquid phase separation under physiological conditions (Fig. 15i and j), and then the MPN membranes made from TA and various metal ions (*e.g.*, Fe^{3+}, Mg^{2+}, and Cs^{+}) were coated onto these coacervates, forming MPN–coacervate composites. The MPNs provided the coacervates with long-term colloidal stability and radical scavenging properties (Fig. 15k). Moreover, MPN–coacervate composites could load diverse cargo (*e.g.*, IgG, GOx, and HRP) and undergo anabolic cascade reactions (Fig. 15l). The surface of MPN–coacervate composites were postmodified with diverse functional ligands for targeted drug delivery. This paradigm of MPN–coacervate composites, featuring a synthetic membrane-bound cytoplasm, holds potential for advancing research in biomimetic materials and diverse biotechnological applications.

4.4. MPN–metal nanoparticle composites

Metal nanoparticles have distinctive physicochemical (*e.g.*, magnetic, catalytic, and optical) properties and have attracted broad use in the fields of physics, chemistry, materials science, and biomedicine.[143] However, metal nanoparticles can also be prone to aggregation, owing to their high surface energy, which can reduce activity.[144] Consequently, precise manipulation of nanoparticle size, shape, and dispersion is essential to achieve optimal performance over extended periods of time. MPNs can prevent nanoparticles from aggregating through spatial confinement, thereby maximizing the potential of metal nanoparticles for diverse applications, such as heterogeneous catalysis, sensors, and antibacterial applications. Unlike metal–organic frameworks, MPNs possess abundant unsaturated coordination sites and can load higher amounts and diverse types of metal nanoparticles. The encapsulation of metal nanoparticles inside MPNs is achieved using two main strategies: coating MPNs on preformed metal nanoparticles or reducing metal salts to nanoparticles within MPNs.

The direct coating of MPNs on metal nanoparticles results in core–shell composites and is generally achieved in two steps. For traditional wet chemical methods, well-defined metal nanoparticles are synthesized by reducing metal salts and subsequently stabilizing them with surfactants (*e.g.*, sodium citrate).[145] Notably, polyphenols can directly reduce noble metal ions (*e.g.*, Au^{3+}, Pd^{2+}, and Ag^{+}) to form metal nanoclusters under controlled conditions, where these nanoclusters are stabilized by surface-bound polyphenols.[146] Polyphenol-mediated metal nanoparticle synthesis offers a flexible and environmentally friendly alternative to traditional methods, which require separate reductants and surfactants, often using toxic components. For instance, a mixture of polyphenols (*e.g.*, TA, EGCG, and GA) with $HAuCl_4$ afforded the reduction of $HAuCl_4$ to gold nanoparticles at room temperature. Subsequently, monodisperse MPN–gold nanoparticle composites ($\sim$35 nm) were successfully synthesized by mixing the as-prepared gold nanoparticles with Fe^{3+} and polyphenols.[101] The MPN shell played a key role in concentrating reactants (*e.g.*, 4-nitrophenol) around the gold nanoparticles through π–π stacking interactions, resulting in improved catalytic performance. The preparation of MPN–gold nanoparticle composites for the reduction of 4-nitrophenol was also be achieved using commercially available Fe powder. The resulting composite displayed catalytic activity and could be recycled up to eight times without a significant decline in catalytic efficiency (Fig. 16a–c).[147]

The second approach of incorporating metal nanoparticles into MPNs is by incubating preformed MPNs with metal salts, facilitating *in situ* reduction and stabilization of the metal nanoparticles. For example, MPNs incorporating diverse metal nanoparticles, including palladium, silver, or gold, were synthesized in an aqueous solution without using toxic chemicals or complex procedures.[148] The synthesis conditions afforded precise control of the size of the formed metal nanoparticles, which retained their high activity (*e.g.*, catalytic or antibacterial) and were recyclable. Similar MPN–silver nanoparticle composites were also used to visualize residual biomolecule patterns, such as proteins, lipids, nucleic acids, and polysaccharides, which are invisible to the naked eye (Fig. 16d).[47] The resulting

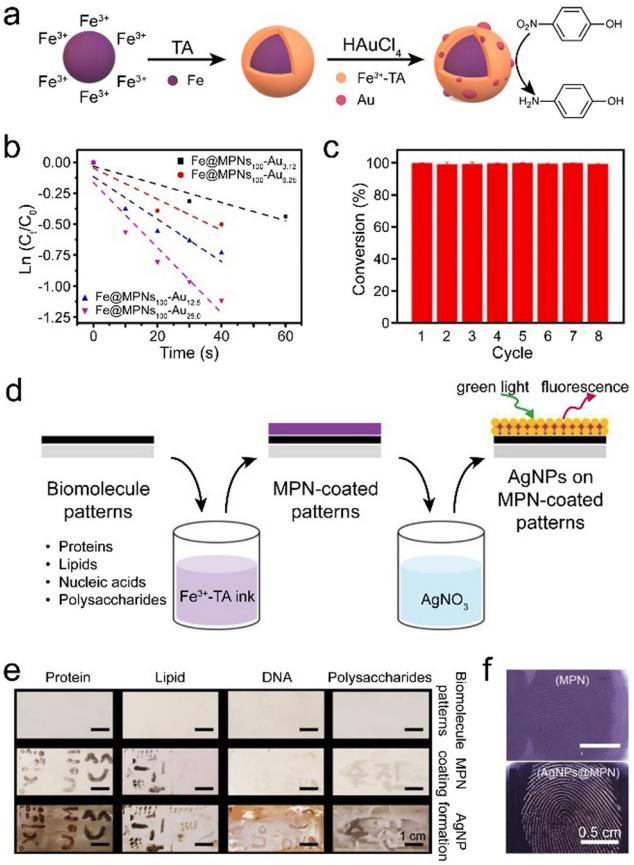

Fig. 16 (a) Schematic illustration of the synthesis of MPN–gold nanoparticle composites. (b) Relationship between ln (C_t/C_0) and reaction time to estimate the effects of gold loading on catalytic efficiency. C_t and C_0 refer to the concentrations of 4-nitrophenol at a specific time and at the initial time, respectively. (c) Catalytic reduction of 4-nitrophenol by MPN–gold nanoparticle composites over eight cycles. (a)–(c) Adapted with permission from ref. 147. Copyright 2022, Elsevier B.V. (d) Schematic illustration of the synthesis of MPN–silver nanoparticle composites to visualize biomolecular patterns. AgNP, silver nanoparticle. (e) Digital photographs of different biomolecular patterns. (f) Reflectance microscopy images of fingerprint patterns. (d)–(f) Adapted with permission from ref. 47. Copyright 2019, Wiley-VCH.

patterns had high-fidelity and enhanced reflectance and fluorescence attributes (Fig. 16e), which allowed identification of latent fingerprints on diverse substrates (Fig. 16f). In addition, a simple strategy for creating a surface-enhanced Raman scattering (SERS) sensor was devised by reducing gold nanoparticles on MPNs *in situ*.[149] The MPN–gold nanoparticle composites had a film-like structure with densely distributed gold nanoparticles, which generated numerous "hot spots" and achieved a SERS effect, exhibiting a limit of detection of as low as 10^{-15} M for 4-mercaptobenzoic acid. This sensor was used as an ultra-sensitive SERS detector of biochemical components in sweat and as a pH nanoprobe to monitor human electrolyte metabolism.

4.5. MPN–oxide composites

Metal oxides, a class of compounds exhibiting tunable electrical, magnetic, and optical properties, are crystalline solids consisting of a metal cation and an oxide anion held together by electrostatic forces, and they play an essential role in various applications.[150,151] To further enhance their performance or introduce new functionalities (*e.g.*, increasing electrochemical surface area and strengthening the oxygen evolution reaction (OER)), metal oxides can be combined with other materials to generate composites (*e.g.*, MPN composites). In principle, the synthesis routes for preparing MPN–metal oxide composites are similar to those used for MPN–metal nanoparticle composites. The first route is *via* the direct interaction between MPNs and metal oxides (*e.g.*, TiO_2, Fe_2O_3, and ZnO). The mechanism relies on the ability of two neighboring phenolic groups from the catechol group to establish bidentate mononuclear chelate complexes and/or bidentate binuclear bridge complexes with these metal oxides.[152] The second route is *via* the generation of a metal oxide inside MPN layers *via* oxidation or decomposition of the precursors.[153] Both routes offer advantages and disadvantages.

MPN coating of metal oxide nanoparticles can be achieved by transforming zeolitic imidazole frameworks (ZIFs; Fig. 17a) into MPNs *via* ligand exchange.[154] The MPN coating protects the metal oxide core from harsh external environments and increases its final performance by synergetic effects. For example, the introduction of Co/Fe-based MPNs on the surface of conductive Fe_2O_3 resulted in approximately a four-fold increase in the electrochemical surface area, and the MPNs demonstrated potential as active sites for OERs (Fig. 17a).[154] Therefore, MPN–Fe_2O_3 composites exhibited substantial improvement in OER performance compared with pristine Fe_2O_3 and ZIF–Fe_2O_3 composites.

$BiVO_4$ is commonly used in photoelectrochemistry and is a promising OER photoanode because of its narrow band gap (~2.4 eV), favorable band edge position, and negligible toxicity.[156] However, it was reported that pristine $BiVO_4$ thin films exhibited a much lower photocurrent density than their theoretical limit of 7.5 mA cm^{-2}, which was attributed to electron–hole recombination. Alternatively, producing MPN–$BiVO_4$ composites has been demonstrated as a strategy to enhance the OER kinetics of $BiVO_4$ photoanodes.[157,158] Thermodynamically, the photo-generated holes from $BiVO_4$ could be transferred directly to the MPN (Co^{2+}–TA) layer. These holes directly oxidized Co^{2+} to Co^{3+} active sites, which subsequently directly oxidized H_2O to O_2. This approach represents a strategy to prepare MPN composite cocatalysts to enhance the thermodynamic and kinetic properties of photoelectrochemical water oxidation.[159]

Nonmetal oxides, such as (porous) silicon dioxide (SiO_2), have emerged as key components in various fields, particularly in biomedicine where the development of stimuli-responsive coatings on mesoporous silica nanoparticle (MSN) surfaces has been used to prevent the leakage of functional cargo.[160,161] Achieving precise control over the response of coatings to specific stimuli is essential, particularly in the design of intricate systems with targeting behavior. For example, the permeability of MPNs can be precisely tuned to achieve specific responses by varying the type of metal ion and its related stoichiometry.[162] Furthermore, by co-loading photoacid

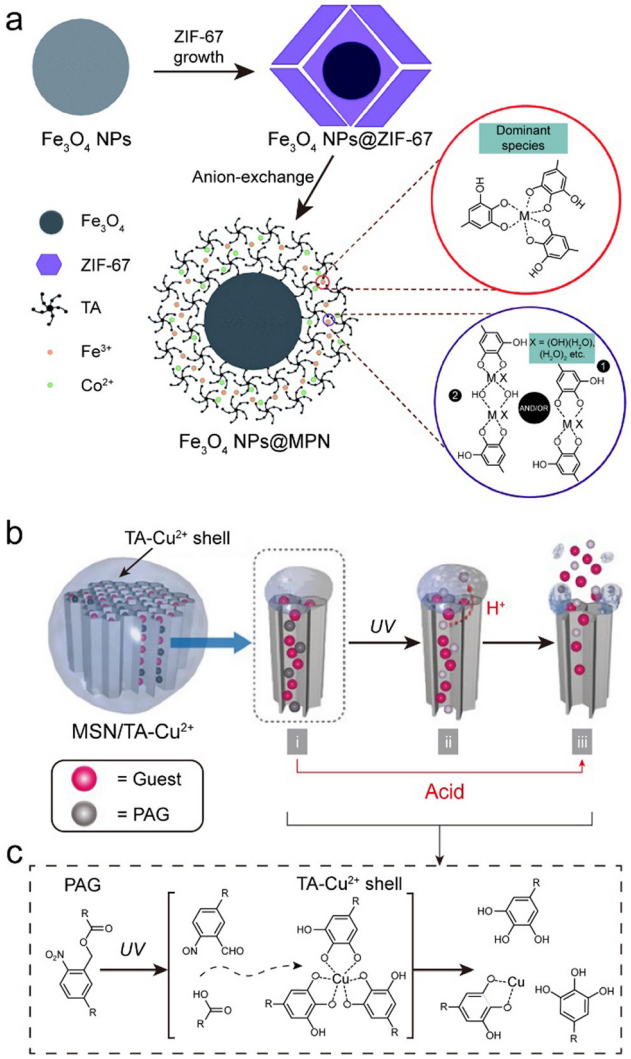

Fig. 17 (a) Schematic illustration of the synthesis MPN–Fe_2O_3 composites. Adapted with permission from ref. 154. Copyright 2019, Royal Society of Chemistry. (b) and (c) Gating activity and adhesion of TA and TA–Cu^{2+} complexes on the surface of MSN. (b) Schematic and (c) mechanism of decomposition of MPNs (Cu^{2+}–TA) by photoacid generators (PAGs) in MPN–MSN composites. (b) and (c) Adapted with permission from ref. 155. Copyright 2017, Wiley-VCH.

generators (*e.g.*, 2-nitrophenyl acetate) inside porous substrates, MPN composites achieved UV responsiveness (Fig. 17b and c).[155] Overall, the combination of porous silica oxides with MPNs may provide avenues for designing smart carrier systems for controlled release.

4.6. MPN–biological entity composites

Biological entities (*e.g.*, cells, bacteria, and viruses) play an essential role in various biological processes but are generally sensitive to the surrounding environmental conditions (*e.g.*, solvent, pH, temperature).[163] MPNs can create a physical barrier between biological entities and the surrounding environment, which increases the viability and tolerance of the biological entities to harsh conditions, including UV radiation and toxins.[117,164,165] Concurrently, the high permeability of MPNs allows nutrient and reactant exchange, enabling the composites to act as efficient bioreactors. For example, under the protection of a selectively degradable MPN (Fe^{3+}–TA) synthetic shell, individual *Saccharomyces cerevisiae* were protected from various external threats (*e.g.*, UV-C radiation, lysozyme, and silver nanoparticles) (Fig. 18a and b).[166] In addition, the MPNs prevented cell proliferation, acting as an artificial sporulation system, as cell proliferation was recovered after shell degradation.

The strategy of forming MPN–biological entity composites can also be applied to protect individual probiotic cells from external factors (*e.g.*, antibiotics) and promote microbial therapy (*e.g.*, amelioration of antibiotic-associated diarrhea (AAD)).[163,167] For example, an MPN single-cell coating of TA and Fe^{3+} was demonstrated to protect both Gram-positive and Gram-negative bacteria against the effects of six clinically relevant antibiotics, and its diverse interactions with antibiotic molecules resulted in the effective adsorption of the antibiotics into the MPN (Fig. 18c–e).[167] MPN–bacteria composites could colonize the gastrointestinal tract of levofloxacin-treated rats, which markedly reduced levofloxacin-induced AAD and alleviated some pre-inflammatory symptoms associated with AAD. Notably, the protective MPN coating ruptured rapidly under acidic conditions, making it suitable for the oral delivery of probiotics to the gastrointestinal tract while retaining bacterial activity. This strategy offers an opportunity to develop progressive bacterial therapeutics for addressing a wide range of diseases.[164]

Photosynthetic microalgae have become a key player in converting CO_2 into various biochemical components. Therefore, regulating microalgae behavior, such as spore formation and germination, is essential for enhancing the yield of valuable metabolites (*e.g.*, proteins, carbohydrates, and carotenoids).[169] The permeable and cytoprotective nature of MPNs enables the encapsulation of microalgae while maintaining their high viability, which can be used to engineer artificial microbial spore formation[170] and control germination and motility. MPN–microalgae composites display precisely regulated cell behaviors.[168] For example, MPN shells were deposited on the surface of *Euglena gracilis* (Eug) through the one-step coordination of TA and Fe^{3+} in a biological buffer to form MPN–microalgae composites (Eug@MPN_x, where x represents the number of MPN coating cycles) (Fig. 18f). The MPN shells minimally influenced the viability and photosynthetic activity of the encapsulated microalgae (Fig. 18g) and significantly modulated the proliferation rate of microalgae cells (Fig. 18h and i). Notably, the MPN shell of the MPN–microalgae composites disassembled in acidic conditions or upon exposure to specific chemical stimulus (*e.g.*, a chelator), allowing rapid degradation (<1 min) of the MPN shell and subsequent revival of the dormant microalgae, which played a pivotal role in controlling the motility of the microalgae (Fig. 18j). Furthermore, MPN–microalgae composites were resistant to environmental stress, including toxic metal ions and antibiotics (Fig. 18k).

4.7. MPN composites with other functional materials

Other functional entities, including carbon materials, nanostructured hybrid materials (*e.g.*, crystalline MOFs), and

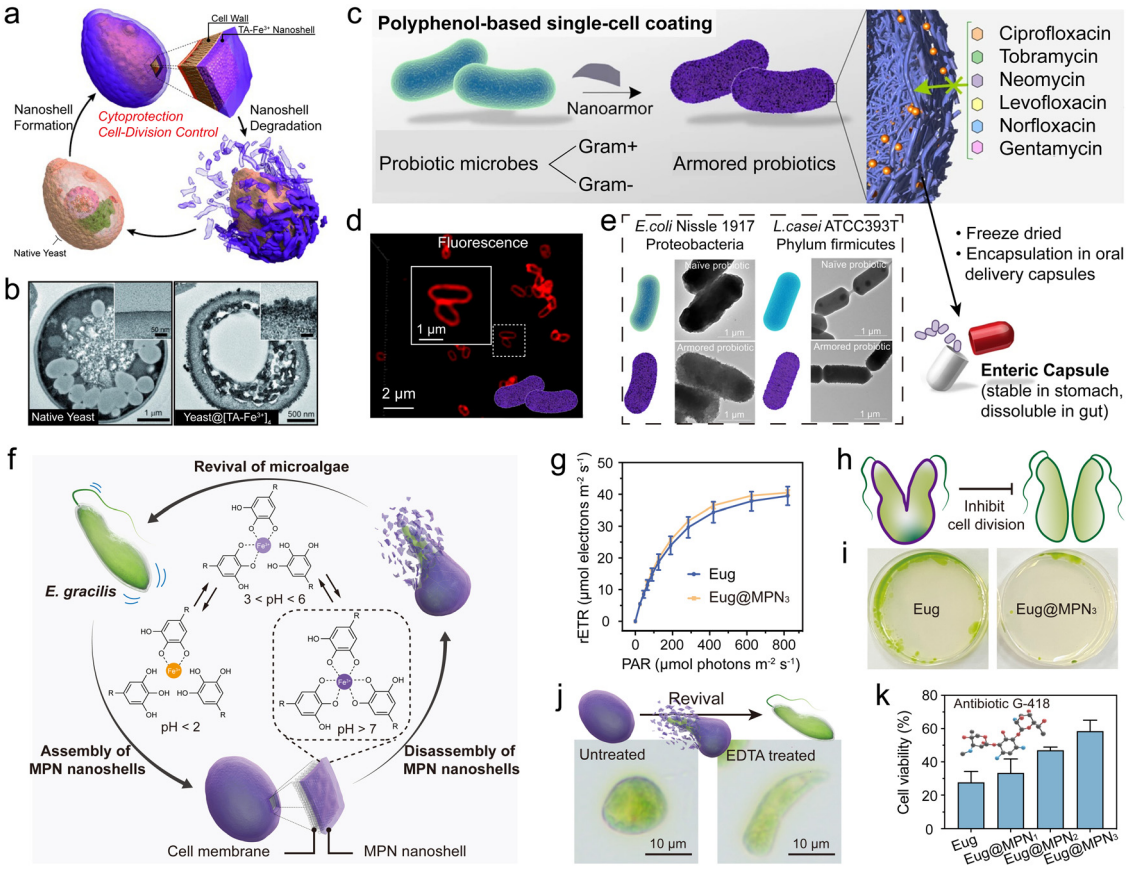

Fig. 18 (a) Schematic illustration of the controlled formation and degradation of MPN–yeast composites. (b) TEM images of native yeast and MPN–yeast composites. (a and b) Adapted with permission from ref. 166. Copyright 2014, Wiley-VCH. (c) MPNs enable rapid, biocompatible single-cell encapsulation, protecting probiotic cells against diverse antibiotics. (d) CLSM images of MPN–bacteria composites. (e) TEM images of bacteria and MPN–bacteria composites. (c)–(e) Adapted with permission from ref. 167. Copyright 2022, Pan *et al.* (f) Schematic of the synthesis of MPN–microalgae composites. (g) Effect of MPNs on the relative electron transport rate (rETR) of Eug. (h) Schematic of MPN–microalgae composites inhibiting the division of microalgae. (i) Effect of MPNs on Eug growth. (j) Microscopy images demonstrating the revival of microalgae. EDTA, ethylenediaminetetraacetic acid. (k) Cytoprotective efficacy of MPN–microalgae composites against antibiotic G-418. (f)–(k) Adapted with permission from ref. 168. Copyright 2023, Li *et al.*, published by Wiley-VCH GmbH.

microneedles, have also been explored to construct MPN composites with new functionalities or enhanced performance.[171,172] For example, the energy-storage mechanism of carbon nanotubes (CNTs) typically relies on the electrical double layer, largely constraining their capacitance. Accordingly, MPNs have been introduced to provide additional high pseudo-capacitance, while the CNTs serve as the conductive substrate for energy-storage applications (Fig. 19a).[171] The mechanical strength of the composites was 17-fold higher than that of the CNTs owing to the strong metal–ligand coordination in the composite. In addition, the MPN–CNT composites exhibited high flexibility and volumetric capacitance, highlighting their potential as energy devices for wearable electronics (Fig. 19b).

Crystalline MOFs are organic–inorganic hybrid materials that have gained significant attention owing to their distinctive characteristics (*e.g.*, high specific surface area, high porosity, and rich chemical tunability). However, when crystalline MOF nanoparticles are incorporated into substrates, issues of MOF particle aggregation and poor interfacial interactions arise, which can lead to nonselective voids and compromise MOF selectivity and structural stability.[11,174] MPN interfacial layers can eliminate these nonselective voids through the interactions between the MPN, crystalline MOF and substrates, thereby enhancing performance.[172,175] Accordingly, MPN–crystalline MOF composite coatings on polymer membranes have wide applications in filtration and separation. For example, an MPN–crystalline MOF composite membrane was fabricated by incorporating hollow MOFs into MPNs *via* an aqueous deposition approach, which led to significantly improved permeability for different organic solvents without sacrificing the rejection performance (Fig. 19c).[173] In particular, the methanol permeability of the MPN–MOF composite membranes was 24.7 L m^{-2} h^{-1} bar^{-1}, significantly outperforming that of pure MPN membranes (9.1 L m^{-2} h^{-1} bar^{-1}, Fig. 19d). Various composites of other crystalline MOFs were also prepared and all exhibited varying degrees of performance enhancement.

Superhydrophilic films with underwater superoleophobicity were designed and prepared by alternately assembling Ti^{4+}–TA network multilayer membrane and ZIF-8 nanocrystals on a

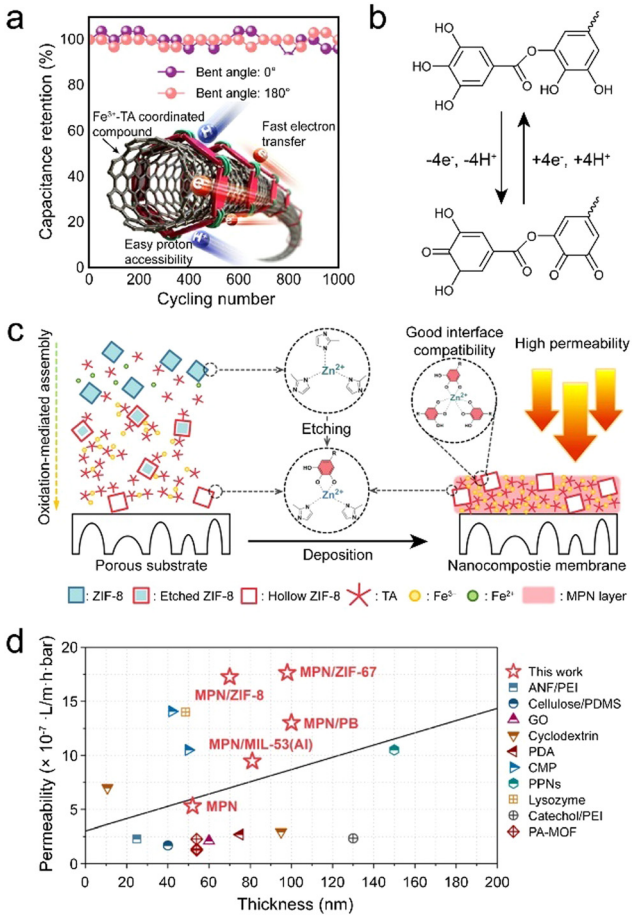

Fig. 19 (a) Metal–phenolic carbon nanocomposite films assembled *via* metal–organic coordination exhibit robustness, flexibility, and stable capacitance during bending. (b) Energy storage mechanism of MPN–CNT composites. (a) and (b) Adapted with permission from ref. 171. Copyright 2017, Wiley-VCH. (c) Schematic of the synthesis of MPN–MOF composite membranes. (d) Comparison of the properties of MPN–MOF composite membranes and membranes in the literature. (c) and (d) Adapted with permission from ref. 173. Copyright 2022, Elsevier B.V.

microfiltration membrane substrate.[176] By integrating their respective advantages of hydrophilicity and hierarchy, the assembled MPN multilayer membrane and ZIF-8 nanocrystal produced a hydrophilic hierarchical structure. The multilayer MPN–MOF composite films showed superhydrophilicity, underwater superoleophobicity, and anti-oil adhesion performance. These properties were beneficial for the rapid penetration of water, achieving high efficiency in separating oil and water and high permeability across various oil/water emulsions. In addition, the prepared superhydrophilic and underwater superoleophobic membranes had good recyclability and antifouling performance, offering significant potential for their practical application in wastewater treatment.

5. Conclusions and perspectives

In this tutorial review, we provided an overview of the multifaceted landscape of MPN composites, covering the building blocks of MPNs, the fundamental aspects of MPN composites, and the advances of MPN composites by focusing on the incorporated functional elements. We now aim, from our perspective, to provide some directions for the future of the field. The versatility in building block choice and assembly conditions of MPNs has made them promising for forming composites, particularly when considering their universal adherence and amorphous nature. Although a wide variety of composites have already been engineered and studied, there are countless variations that can be created in attempting to address scientific and application-focused challenges. Below, we highlight a few materials, design strategies, and gaps in the literature that should be particularly interesting for future MPN composite research.

Materials of interest

Commercial polyphenols are primarily sourced from natural plants (*e.g.*, gallnuts), where multiple phenolic ligands often coexist, which can restrict the ordered arrangement of the coordination network and consequently impact the properties of the MPN composites. Exploring highly efficient strategies to extract and purify biomass-derived phenolic ligands with fewer by-products would help provide a deeper understanding and the specific engineering of metal–phenolic coordination chemistry. Moreover, only a small fraction of polyphenol types have been used to date, thus exploring additional natural and synthetic phenolic ligands that feature desired functionalities (*e.g.*, conductivity, therapeutic effects) holds promise for various applications across diverse fields.

The number (and diversity) of functional components that have been incorporated into MPNs is also considerably fewer than those examined with other metal–organic systems such as crystalline MOFs. Exploring the incorporation of new functional components (*e.g.*, quantum dots, halide perovskites) is expected to expand the library and potential of MPN composites and extend the synergies between MPNs and other functional materials. Components with specific optical, electrical, and catalytic properties are yet to be extensively explored in combination with MPNs, and the tunable redox properties and optical properties offer diverse opportunities to engineer performance.

A distinct benefit of MPNs is their mild synthesis conditions that are generally applied to biological entities—an area of intense interest for MPN composites. However, there is a range of biological entities that have not been incorporated with MPNs, and which are yet to be examined. There is still a need to move beyond studies that simply demonstrate that MPNs are protective. Using genetically engineered organisms, synthetic biology, and other emerging approaches should further expand the potential of MPN composites in biotechnology applications.

Notably, many practical applications require multiple properties and functionalities to be included in a single composite (*e.g.*, efficient drug delivery requires imaging, targeting, and responsive release). Therefore, the inclusion of numerous functional components within MPNs is expected to realize these applications. Moreover, functional components that

produce triggers can then change MPNs or trigger a response. This requires a more in-depth analysis of the various components and the different ways that they can interact.

Finally, creating nanostructured materials using MPN composites as precursors offers a means to engineer functional materials with different properties.[177] For example, the thermal transformation of MPN composites allows their carbonization into multi-metal-doped carbon materials, offering promise for applications ranging from environmental remediation to catalysis. This strategy could also potentially be applicable to creating composites based on metal oxides, metal chalcogenides, and metal phosphides. Exploring how the MPN composite properties (*e.g.*, pore size, metal density, ligand length) influence the final materials will further allow for the rational design of 2D and 3D functional materials.

Design strategies

Processing composites into functional structures on the macroscopic scale (*e.g.*, membranes, monoliths) is generally challenging yet required for the practical applications of most materials. The mild synthesis conditions involved in forming MPN composites and the amenability of MPNs to a wide range of solvents offer a variety of routes for processing MPN composites. For example, the use of MPN composites in innovative manufacturing techniques (*e.g.*, 3D bioprinting) will offer a range of new opportunities.

Tuning the porosity of MPN composites could enhance their performance by controlling how reagents diffuse in and out of the composites for target applications. Engineering the pore size and geometry are central research topics for crystalline MOF composites and have led to significant increases in their surface area over the past three decades.[178] The pore size of MPN composites can be tuned by adjusting the metal-to-ligand ratio, precursor type and concentration. However, fabricating MPN composites that feature micropores, narrow pore size distributions, or high surface areas remains challenging, yet essential for separation and energy applications.

MPNs display a wide range of interactive forces but hydrogen bonding, chelation, and hydrophobic interactions are primarily used in their assembly. Other interactions (*e.g.*, π–anion interactions) and careful planning related to which interactions should be used to govern the specific properties of composites (*e.g.*, stability, responsiveness, photon or electron transport) should allow for efficiency gains in already existing MPN composites and the design of new composites.

Gaps in the literature

As MPNs are amorphous and display a wide range of interactive forces, there are significant gaps in the literature relating to the structure and properties of MPNs by themselves and MPN composites, when compared to materials such as crystalline MOFs. Therefore, significant research, novel characterization techniques, and advanced techniques, such as synchrotron radiation, are all needed to uncover fundamental understanding related to MPNs and their interactions. Moreover, simulations and modeling of the energetics involved, assembly processes, and response to stimuli can provide avenues for the rational design of MPN composites. The integration of machine learning into MPN composite design is also expected to accelerate the discovery and optimization of emerging MPN composites. Conventional methods of exploring new composites often rely on empirical approaches, which require extensive experimental work to obtain MPN composite materials with desired properties. Machine learning models have facilitated the development of crystalline MOF materials.[179] Therefore, such high-throughput computation provides opportunities to extensively evaluate metal ions and phenolic ligands for predicting or generating MPN composite materials for specific applications.

We anticipate that MPN composites will play a pivotal role in shaping the landscape of composite materials and advanced technologies, as a handful of MPN composites are already on the market. Continuous study and development will lead to groundbreaking advances in various scientific fields and industrial applications.

Data availability

No primary research results, software or code have been included and no new data were generated or analysed as part of this review.

Conflicts of interest

J. J. R. is the inventor of SWIFF and has a financial interest in it.

Acknowledgements

This research was funded in part by the National Health and Medical Research Council (GNT2016732, F. C.). This research was also supported by an Australian Research Council (ARC) Discovery Project scheme (F. C., DP210103114). Z. L. acknowledges The University of Melbourne for an Early Career Researcher grant. J. J. R. is a recipient of a Future Fellowship from the ARC (FT210100669). J. Z. acknowledges the Fundamental Research Funds for the Central Universities and the Opening Project of Key Laboratory of Leather Chemistry and Engineering (Sichuan University) of Ministry of Education.

References

1 G. W. Peterson, D. T. Lee, H. F. Barton, T. H. Epps and G. N. Parsons, *Nat. Rev. Mater.*, 2021, **6**, 605–621.
2 M. R. Begley, D. S. Gianola and T. R. Ray, *Science*, 2019, **364**, eaav4299.
3 A. Kinloch, J. Suhr, J. Lou, R. J. Young and P. M. Ajayan, *Science*, 2018, **362**, 547–553.
4 H. Furukawa, K. E. Cordova, M. O'Keeffe and O. M. Yaghi, *Science*, 2013, **341**, 1230444.
5 H.-C. Zhou, J. R. Long and O. M. Yaghi, *Chem. Rev.*, 2012, **112**, 673–674.

6 R. F. Mendes, F. Figueira, J. P. Leite, L. Gales and F. A. A. Paz, *Chem. Soc. Rev.*, 2020, **49**, 9121–9153.
7 M. Gutiérrez, Y. Zhang and J.-C. Tan, *Chem. Rev.*, 2022, **122**, 10438–10483.
8 K. Jayaramulu, S. Mukherjee, D. M. Morales, D. P. Dubal, A. K. Nanjundan, A. Schneemann, J. Masa, S. Kment, W. Schuhmann and M. Otyepka, *Chem. Rev.*, 2022, **122**, 17241–17338.
9 Q. Yang, Q. Xu and H.-L. Jiang, *Chem. Soc. Rev.*, 2017, **46**, 4774–4808.
10 W. Liang, P. Wied, F. Carraro, C. J. Sumby, B. Nidetzky, C.-K. Tsung, P. Falcaro and C. J. Doonan, *Chem. Rev.*, 2021, **121**, 1077–1129.
11 M. Kalaj, K. C. Bentz, S. Ayala, J. M. Palomba, K. S. Barcus, Y. Katayama and S. M. Cohen, *Chem. Rev.*, 2020, **120**, 8267–8302.
12 L. Chen, R. Luque and Y. Li, *Chem. Soc. Rev.*, 2017, **46**, 4614–4630.
13 Q.-L. Zhu and Q. Xu, *Chem. Soc. Rev.*, 2014, **43**, 5468–5512.
14 H. Ejima, J. J. Richardson, K. Liang, J. P. Best, M. P. van Koeverden, G. K. Such, J. Cui and F. Caruso, *Science*, 2013, **341**, 154–157.
15 Z. Lin, J. J. Richardson, J. Zhou and F. Caruso, *Nat. Rev. Chem.*, 2023, **7**, 273–286.
16 J. Guo, B. L. Tardy, A. J. Christofferson, Y. Dai, J. J. Richardson, W. Zhu, M. Hu, Y. Ju, J. Cui, R. R. Dagastine, I. Yarovsky and F. Caruso, *Nat. Nanotechnol.*, 2016, **11**, 1105–1111.
17 H. Geng, Q.-Z. Zhong, J. Li, Z. Lin, J. Cui, F. Caruso and J. Hao, *Chem. Rev.*, 2022, **122**, 11432–11473.
18 J. Zhou, Z. Lin, Y. Ju, M. A. Rahim, J. J. Richardson and F. Caruso, *Acc. Chem. Res.*, 2020, **53**, 1269–1278.
19 D. Wu, J. Zhou, M. N. Creyer, W. Yim, Z. Chen, P. B. Messersmith and J. V. Jokerst, *Chem. Soc. Rev.*, 2021, **50**, 4432–4483.
20 L. Q. Xu, K.-G. Neoh and E.-T. Kang, *Prog. Polym. Sci.*, 2018, **87**, 165–196.
21 Z. Lin, J. Zhou, C. Cortez-Jugo, Y. Han, Y. Ma, S. Pan, E. Hanssen, J. J. Richardson and F. Caruso, *J. Am. Chem. Soc.*, 2019, **142**, 335–341.
22 L. Xie, J. Li, G. Wang, W. Sang, M. Xu, W. Li, J. Yan, B. Li, Z. Zhang and Q. Zhao, *J. Am. Chem. Soc.*, 2022, **144**, 787–797.
23 Z. Guo, J. J. Richardson, B. Kong and K. Liang, *Sci. Adv.*, 2020, **6**, eaaz0330.
24 J. Guo, Y. Ping, H. Ejima, K. Alt, M. Meissner, J. J. Richardson, Y. Yan, K. Peter, D. Von Elverfeldt, C. E. Hagemeyer and F. Caruso, *Angew. Chem., Int. Ed.*, 2014, **53**, 5546–5551.
25 L. Bravo, *Nutr. Rev.*, 1998, **56**, 317–333.
26 S. Quideau, D. Deffieux, C. Douat-Casassus and L. Pouységu, *Angew. Chem., Int. Ed.*, 2011, **50**, 586–621.
27 D. P. Makris, G. Boskou and N. K. Andrikopoulos, *J. Food Compos. Anal.*, 2007, **20**, 125–132.
28 H. Lee, W. I. Kim, W. Youn, T. Park, S. Lee, T. S. Kim, J. F. Mano and I. S. Choi, *Adv. Mater.*, 2018, **30**, 1805091.
29 V. Kavitha and B. Kandasubramanian, *SN Appl. Sci.*, 2020, **2**, 1081.
30 J. Guo, T. Suma, J. J. Richardson and H. Ejima, *ACS Biomater. Sci. Eng.*, 2019, **5**, 5578–5596.
31 Y. Guo, Q. Sun, F. G. Wu, Y. Dai and X. Chen, *Adv. Mater.*, 2021, **33**, 2007356.
32 Y. Ju, J. Cui, H. Sun, M. Müllner, Y. Dai, J. Guo, N. Bertleff-Zieschang, T. Suma, J. J. Richardson and F. Caruso, *Biomacromolecules*, 2016, **17**, 2268–2276.
33 B. Cheng, J. Yu, T. Arisawa, K. Hayashi, J. J. Richardson, Y. Shibuta and H. Ejima, *Nat. Commun.*, 2022, **13**, 1892.
34 C.-J. Kim, F. Ercole, J. Chen, S. Pan, Y. Ju, J. F. Quinn and F. Caruso, *J. Am. Chem. Soc.*, 2022, **144**, 503–514.
35 B. L. Tardy, J. J. Richardson, V. Nithipipat, K. Kempe, J. Guo, K. L. Cho, M. A. Rahim, H. Ejima and F. Caruso, *Biomacromolecules*, 2019, **20**, 1421–1428.
36 B. Cheng, S. Lu, W. Liao, C. Wang, J. J. Richardson and H. Ejima, *Nanoscale*, 2022, **14**, 14466–14470.
37 S. Oliver, O. Vittorio, G. Cirillo and C. Boyer, *Polym. Chem.*, 2016, **7**, 1529–1544.
38 R. Hlushko, H. Hlushko and S. A. Sukhishvili, *Polym. Chem.*, 2018, **9**, 506–516.
39 E. Khare, N. Holten-Andersen and M. J. Buehler, *Nat. Rev. Mater.*, 2021, **6**, 421–436.
40 W. Xu, S. Pan, B. B. Noble, J. Chen, Z. Lin, Y. Han, J. Zhou, J. J. Richardson, I. Yarovsky and F. Caruso, *Angew. Chem., Int. Ed.*, 2022, **61**, e202208037.
41 T. Liu, M. Zhang, W. Liu, X. Zeng, X. Song, X. Yang, X. Zhang and J. Feng, *ACS Nano*, 2018, **12**, 3917–3927.
42 X. Zhang, L. Chen, C. Zhang and L. Liao, *ACS Appl. Mater. Interfaces*, 2021, **13**, 18175–18183.
43 H. Mei, H. Liu, C. Sha, Q. Lv, Q. Song, L. Jiang, E. Tian, Z. Gao, J. Li and J. Zhou, *ACS Appl. Mater. Interfaces*, 2024, **16**, 13573–13584.
44 S. Spoljaric, Y. Ju and F. Caruso, *Chem. Mater.*, 2021, **33**, 1099–1115.
45 H. Wang, D. Wang, J. Yu, Y. Zhang and Y. Zhou, *Biomater. Sci.*, 2022, **10**, 5786–5808.
46 H. J. Kim, D. G. Kim, H. Yoon, Y. S. Choi, J. Yoon and J. C. Lee, *Adv. Mater. Interfaces*, 2015, **2**, 1500298.
47 G. Yun, J. J. Richardson, M. Capelli, Y. Hu, Q. A. Besford, A. C. G. Weiss, H. Lee, I. S. Choi, B. C. Gibson, P. Reineck and F. Caruso, *Adv. Funct. Mater.*, 2019, **30**, 1905805.
48 Y. Han, Z. Lin, J. Zhou, G. Yun, R. Guo, J. J. Richardson and F. Caruso, *Angew. Chem., Int. Ed.*, 2020, **59**, 15618–15625.
49 H. Cory, S. Passarelli, J. Szeto, M. Tamez and J. Mattei, *Front. Nutr.*, 2018, **5**, 370438.
50 H. Wang, C. Wang, Y. Zou, J. Hu, Y. Li and Y. Cheng, *Giant*, 2020, **3**, 100022.
51 C. Chen, M. Lin, C. Wahl, Y. Li, W. Zhou, Z. Wang, Y. Zhang and C. A. Mirkin, *J. Am. Chem. Soc.*, 2023, **145**, 7974–7982.
52 W. Xu, S. Pan, B. B. Noble, Z. Lin, S. Kaur Bhangu, C.-J. Kim, J. Chen, Y. Han, I. Yarovsky and F. Caruso, *Angew. Chem., Int. Ed.*, 2023, **62**, e202302448.

53 H. Lee, D. T. Nguyen, N. Kim, S. Y. Han, Y. J. Hong, G. Yun, B. J. Kim and I. S. Choi, *ACS Appl. Mater. Interfaces*, 2021, **13**, 52385–52394.
54 Q. Z. Zhong, S. Li, J. Chen, K. Xie, S. Pan, J. J. Richardson and F. Caruso, *Angew. Chem., Int. Ed.*, 2019, **58**, 12563–12568.
55 M. A. Rahim, M. Björnmalm, N. Bertleff-Zieschang, Q. Besford, S. Mettu, T. Suma, M. Faria and F. Caruso, *Adv. Mater.*, 2017, **29**, 1606717.
56 R. Yu, H. Chen, J. He, Z. Zhang, J. Zhou, Q. Zheng, Z. Fu, C. Lu, Z. Lin, F. Caruso and X. Zhang, *Adv. Mater.*, 2024, **36**, 2307680.
57 Z. Fu, Y. Zhang, X. Chen, N. Wang, R. Ma, X. Luo, X. Pan, Y. Yang and W. Xue, *Adv. Funct. Mater.*, 2023, **33**, 2211869.
58 Z. Guo, T. Liu, W. Gao, C. Iffelsberger, B. Kong and M. Pumera, *Adv. Mater.*, 2023, **35**, 2210994.
59 G. Choi, E. I. Fitriasari and C. Park, *ACS Nano*, 2021, **15**, 14580–14586.
60 J. Chen, J. Li, J. Zhou, Z. Lin, F. Cavalieri, E. Czuba-Wojnilowicz, Y. Hu, A. Glab, Y. Ju, J. J. Richardson and F. Caruso, *ACS Nano*, 2019, **13**, 11653–11664.
61 G. Lin, J. J. Richardson, H. Ahmed, Q. A. Besford, A. J. Christofferson, S. Beyer, Z. Lin, A. R. Rezk, M. Savioli, J. Zhou, C. F. McConville, C. Cortez-Jugo, L. Y. Yeo and F. Caruso, *Adv. Mater.*, 2021, **33**, 2006177.
62 Z. Wang, J. Gao, J. Zhou, J. Gong, L. Shang, H. Ye, F. He, S. Peng, Z. Lin, Y. Li and F. Caruso, *Adv. Mater.*, 2023, **35**, 2209015.
63 X. Sun and T. D. James, *Chem. Rev.*, 2015, **115**, 8001–8037.
64 Y. Li, Y. Miao, L. Yang, Y. Zhao, K. Wu, Z. Lu, Z. Hu and J. Guo, *Adv. Sci.*, 2022, **9**, 2202684.
65 J. J. Richardson, W. Liao, J. Li, B. Cheng, C. Wang, T. Maruyama, B. L. Tardy, J. Guo, L. Zhao, W. Aw and H. Ejima, *Sci. Rep.*, 2022, **12**, 2071.
66 L. Chen, M. Peng, H. Li, J. Zhou, W. He, R. Hu, F. Ye, Y. Li, L. Shi and Y. Liu, *Adv. Mater.*, 2024, **36**, 2306376.
67 S. Yang, H. Zhang, X. Sun, J. Bai and J. Zhang, *ACS Nano*, 2024, **18**, 5847–5863.
68 S. Pan, J. J. Richardson, A. J. Christofferson, Q. A. Besford, T. Zheng, B. J. Wood, X. Duan, M. J. Jara Fornerod, C. F. McConville, I. Yarovsky, S. Guldin, L. Jiang and F. Caruso, *J. Am. Chem. Soc.*, 2021, **143**, 9972–9981.
69 W. Xu, Z. Lin, S. Pan, J. Chen, T. Wang, C. Cortez-Jugo and F. Caruso, *Angew. Chem., Int. Ed.*, 2023, **62**, e202312925.
70 Z. Wang, Y. Guo, Y. Fan, J. Chen, H. Wang, M. Shen and X. Shi, *Adv. Mater.*, 2022, **34**, 2107009.
71 C. Xu, C. Peng, X. Yang, R. Zhang, Z. Zhao, B. Yan, J. Zhang, J. Gong, X. He, R. T. K. Kwok, J. W. Y. Lam and B. Z. Tang, *Adv. Sci.*, 2022, **9**, 2104997.
72 J. H. Park, S. Choi, H. C. Moon, H. Seo, J. Y. Kim, S.-P. Hong, B. S. Lee, E. Kang, J. Lee and D. H. Ryu, *Sci. Rep.*, 2017, **7**, 6980.
73 Q.-Z. Zhong, S. Pan, M. A. Rahim, G. Yun, J. Li, Y. Ju, Z. Lin, Y. Han, Y. Ma, J. J. Richardson and F. Caruso, *ACS Appl. Mater. Interfaces*, 2018, **10**, 33721–33729.
74 C. Maerten, L. Lopez, P. Lupattelli, G. Rydzek, S. Pronkin, P. Schaaf, L. Jierry and F. Boulmedais, *Chem. Mater.*, 2017, **29**, 9668–9679.
75 G. Yun, W. Youn, H. Lee, S. Y. Han, M. B. Oliveira, H. Cho, F. Caruso, J. F. Mano and I. S. Choi, *Chem. Mater.*, 2020, **32**, 7746–7753.
76 B. J. Kim, S. Han, K.-B. Lee and I. S. Choi, *Adv. Mater.*, 2017, **29**, 1700784.
77 J. Chen, S. Spoljaric, A. Calatayud-Sanchez, Y. Alvarez-Braña and F. Caruso, *ACS Appl. Mater. Interfaces*, 2023, **15**, 48050–48059.
78 Z. Liu, Z. Le, L. Lu, Y. Zhu, C. Yang, P. Zhao, Z. Wang, J. Shen, L. Liu and Y. Chen, *Nanoscale*, 2019, **11**, 9410–9421.
79 Y. Li, X. Cheng, X. Zhang, Z. Ma, C. Deng, C. Liu and X. Jian, *Chem. Eng. J.*, 2024, **486**, 150234.
80 F. Centurion, M. M. Hassan, J. Tang, F.-M. Allioux, S. Chakraborty, R. Chen, G. Mao, N. Kumar, K. Kalantar-Zadeh and M. A. Rahim, *Nanoscale*, 2022, **14**, 14760–14769.
81 O. Mazaheri, A. Zavabeti, R. V. McQuillan, Z. Lin, M. S. Alivand, E. Della Gaspera, D. Chen, F. Caruso, H. Suter and K. A. Mumford, *Chem. Mater.*, 2023, **35**, 7800–7813.
82 J. Kang, G. Bai, S. Ma, X. Liu, Z. Ma, X. Guo, X. Wang, B. Dai, F. Zhou and X. Jia, *Adv. Mater. Interfaces*, 2019, **6**, 1801789.
83 P. Zhang, L. Wang, S. Yang, J. A. Schott, X. Liu, S. M. Mahurin, C. Huang, Y. Zhang, P. F. Fulvio and M. F. Chisholm, *Nat. Commun.*, 2017, **8**, 15020.
84 S. Wang, C. M. McGuirk, A. d'Aquino, J. A. Mason and C. A. Mirkin, *Adv. Mater.*, 2018, **30**, 1800202.
85 F. Liu, X. He, H. Chen, J. Zhang, H. Zhang and Z. Wang, *Nat. Commun.*, 2015, **6**, 8003.
86 J. Chen, S. Pan, J. Zhou, Z. Lin, Y. Qu, A. Glab, Y. Han, J. J. Richardson and F. Caruso, *Adv. Mater.*, 2022, **34**, 2108624.
87 Y. Dai, Z. Yang, S. Cheng, Z. Wang, R. Zhang, G. Zhu, Z. Wang, B. C. Yung, R. Tian and O. Jacobson, *Adv. Mater.*, 2018, **30**, 1704877.
88 M. A. Rahim, M. Björnmalm, T. Suma, M. Faria, Y. Ju, K. Kempe, M. Müllner, H. Ejima, A. D. Stickland and F. Caruso, *Angew. Chem., Int. Ed.*, 2016, **55**, 13803–13807.
89 M. A. Rahim, Y. Hata, M. Björnmalm, Y. Ju and F. Caruso, *Small*, 2018, **14**, 1801202.
90 M. Bjornmalm, L. M. Wong, J. P. Wojciechowski, J. Penders, C. C. Horgan, M. A. Booth, N. G. Martin, S. Sattler and M. M. Stevens, *Chem. Sci.*, 2019, **10**, 10179–10194.
91 M. Li, H. Wang, J. Hu, J. Hu, S. Zhang, Z. Yang, Y. Li and Y. Cheng, *Chem. Mater.*, 2019, **31**, 7678–7685.
92 Z. Li, X. Huang, L. Lin, Y. Jiao, C. Zhou and Z. Liu, *Chem. Eng. J.*, 2021, **419**, 129488.
93 Y. Liang, Z. Li, Y. Huang, R. Yu and B. Guo, *ACS Nano*, 2021, **15**, 7078–7093.
94 Y. Li, R. Fu, Z. Duan, C. Zhu and D. Fan, *Bioact. Mater.*, 2022, **9**, 461–474.
95 G. Shen, R. Xing, N. Zhang, C. Chen, G. Ma and X. Yan, *ACS Nano*, 2016, **10**, 5720–5729.
96 F. Raza, H. Zafar, M. W. Khan, A. Ullah, A. U. Khan, A. Baseer, R. Fareed and M. Sohail, *Mater. Adv.*, 2022, **3**, 2268–2290.

97 P. Liu, X. Shi, S. Zhong, Y. Peng, Y. Qi, J. Ding and W. Zhou, *Biomater. Sci.*, 2021, **9**, 2825–2849.
98 C. Wang, H. Sang, Y. Wang, F. Zhu, X. Hu, X. Wang, X. Wang, Y. Li and Y. Cheng, *Nano Lett.*, 2018, **18**, 7045–7051.
99 F. Huang, X. Jiang, M. A. Sallam, X. Zhang and W. He, *AAPS PharmSciTech*, 2022, **23**, 76.
100 Y. Shen, S. A. Yuk, S. Kwon, H. Tamam, Y. Yeo and B. Han, *J. Controlled Release*, 2023, **357**, 484–497.
101 T. Zeng, X. Zhang, Y. Guo, H. Niu and Y. Cai, *J. Mater. Chem. A*, 2014, **2**, 14807–14811.
102 Q. Wang, Y. Xu, R. Xue, J. Fan, H. Yu, J. Guan, H. Wang, M. Li, W. Yu, Z. Xie, R. Qi, X. Jia and B. Han, *Small*, 2022, **18**, 2104660.
103 C. Guo, J. Cao and Z. Chen, *Appl. Surf. Sci.*, 2022, **605**, 154747.
104 B. Yang, S. Zhou, J. Zeng, L. Zhang, R. Zhang, K. Liang, L. Xie, B. Shao, S. Song, G. Huang, D. Zhao, P. Chen and B. Kong, *Nano Res.*, 2020, **13**, 1013–1019.
105 Y. Gao, S. C. Yang, M. H. Zhu, X. D. Zhu, X. Luan, X. L. Liu, X. Lai, Y. Yuan, Q. Lu, P. Sun, J. F. Lovell, H. Z. Chen and C. Fang, *Small*, 2021, **17**, 2100789.
106 Y. Ping, J. Guo, H. Ejima, X. Chen, J. J. Richardson, H. Sun and F. Caruso, *Small*, 2015, **11**, 2032–2036.
107 A. Ali, R. Javed, S. Farhangi, T. Shah, S. Ullah, N. Ul Ain, T. Liu, Z. Guo, I. Lynch, F. Raza, P. Zhang and Y. Rui, *J. Drug Delivery Sci. Technol.*, 2023, **84**, 104536.
108 S. Liu, X. Xu, J. Ye, J. Wang, Q. Wang, Z. Liu, J. Xu and Y. Fu, *Chem. Eng. J.*, 2023, **456**, 140892.
109 P. Cai, X. Zhang, M. Wang, Y.-L. Wu and X. Chen, *ACS Nano*, 2018, **12**, 5078–5084.
110 M. A. Boles, D. Ling, T. Hyeon and D. V. Talapin, *Nat. Mater.*, 2016, **15**, 141–153.
111 A. Albanese, P. S. Tang and W. C. Chan, *Annu. Rev. Biomed. Eng.*, 2012, **14**, 1–16.
112 Y. Ju, Q. Dai, J. Cui, Y. Dai, T. Suma, J. J. Richardson and F. Caruso, *ACS Appl. Mater. Interfaces*, 2016, **8**, 22914–22922.
113 W. Zhang, Q. A. Besford, A. J. Christofferson, P. Charchar, J. J. Richardson, A. Elbourne, K. Kempe, C. E. Hagemeyer, M. R. Field, C. F. McConville, I. Yarovsky and F. Caruso, *Nano Lett.*, 2020, **20**, 2660–2666.
114 Y. Wang, T. Wei, Y. Qu, Y. Zhou, Y. Zheng, C. Huang, Y. Zhang, Q. Yu and H. Chen, *ACS Appl. Mater. Interfaces*, 2019, **12**, 21283–21291.
115 Z. Lin, J. Zhou, Y. Qu, S. Pan, Y. Han, R. P. M. Lafleur, J. Chen, C. Cortez-Jugo, J. J. Richardson and F. Caruso, *Angew. Chem., Int. Ed.*, 2021, **60**, 24968–24975.
116 J. Chen, C. Cortez-Jugo, C.-J. Kim, Z. Lin, T. Wang, R. De Rose, W. Xu, Z. Wang, Y. Gu and F. Caruso, *Angew. Chem., Int. Ed.*, 2024, **63**, e202319583.
117 Z. Wu, J. Zhou, C. I. Nkanga, Z. Jin, T. He, R. M. Borum, W. Yim, J. Zhou, Y. Cheng and M. Xu, *ACS Appl. Mater. Interfaces*, 2022, **14**, 13692–13702.
118 Z. Yang, Y. Yang, K. Xiong, J. Wang, H. Lee and N. Huang, *Chem. Mater.*, 2018, **30**, 5220–5226.
119 Q. Chen, Q. Qian, H. Xu, H. Zhou, L. Chen, N. Shao, K. Zhang, T. Chen, H. Tian and Z. Zhang, *ACS Nano*, 2024, **18**, 8885–8905.
120 A. M. Vargason, A. C. Anselmo and S. Mitragotri, *Nat. Biomed. Eng.*, 2021, **5**, 951–967.
121 M. T. Manzari, Y. Shamay, H. Kiguchi, N. Rosen, M. Scaltriti and D. A. Heller, *Nat. Rev. Mater.*, 2021, **6**, 351–370.
122 H. Xiong, C. Wang, Z. Wang, Z. Jiang, J. Zhou and J. Yao, *J. Controlled Release*, 2019, **309**, 145–157.
123 X. Li, Z. Duan, X. Chen, D. Pan, Q. Luo, L. Gu, G. Xu, Y. Li, H. Zhang and Q. Gong, *Adv. Mater.*, 2023, **35**, 2300548.
124 C.-J. Kim, F. Ercole, Y. Ju, S. Pan, J. Chen, Y. Qu, J. F. Quinn and F. Caruso, *Chem. Mater.*, 2021, **33**, 8477–8488.
125 J. Yang, L. Wang, A. Xie, X. Dai, Y. Yan and J. Dai, *Surf. Coat. Technol.*, 2020, **389**, 125630.
126 M. Obaid, H. O. Mohamed, A. B. Alayande, Y. Kang, N. Ghaffour and I. S. Kim, *Sep. Purif. Technol.*, 2021, **272**, 118954.
127 Z. Bai, K. Jia, S. Zhang, G. Lin, Y. Huang and X. Liu, *Adv. Funct. Mater.*, 2022, **32**, 2204612.
128 C.-J. Kim, F. Ercole, E. Goudeli, S. K. Bhangu, J. Chen, M. Faria, J. F. Quinn and F. Caruso, *Chem. Mater.*, 2022, **34**, 7468–7480.
129 Y. Wen, X. Yang, Y. Li, L. Yan, Y. Zhao and L. Shao, *Sep. Purif. Technol.*, 2023, **320**, 124225.
130 Y. Tian, M. V. Tirrell and J. L. LaBelle, *Adv. Healthcare Mater.*, 2022, **11**, 2102600.
131 R. A. Sheldon and S. van Pelt, *Chem. Soc. Rev.*, 2013, **42**, 6223–6235.
132 L. Guo, S. Zhong, P. Liu, M. Guo, J. Ding and W. Zhou, *Small*, 2022, **18**, 2202604.
133 X. Tan, R. Sheng, Z. Liu, W. Li, R. Yuan, Y. Tao, N. Yang and L. Ge, *Small*, 2023, **20**, 2305325.
134 L. Jiang, Y. Zeng, H. Li, Z. Lin, H. Liu, J. J. Richardson, Z. Gao, D. Wu, L. Liu, F. Caruso and J. Zhou, *J. Am. Chem. Soc.*, 2023, **145**, 24108–24115.
135 T. D. Brown, K. A. Whitehead and S. Mitragotri, *Nat. Rev. Mater.*, 2020, **5**, 127–148.
136 Z. He, T. Nie, Y. Hu, Y. Zhou, J. Zhu, Z. Liu, L. Liu, K. W. Leong, Y. Chen and H.-Q. Mao, *J. Controlled Release*, 2020, **318**, 86–97.
137 D. A. Richards, A. Maruani and V. Chudasama, *Chem. Sci.*, 2017, **8**, 63–77.
138 L. Hao, T. Li, L. Wang, X. Shi, Y. Fan, C. Du and Y. Wang, *Bioact. Mater.*, 2021, **6**, 3125–3135.
139 Y. Xu, Y. Guo, C. Zhang, M. Zhan, L. Jia, S. Song, C. Jiang, M. Shen and X. Shi, *ACS Nano*, 2022, **16**, 984–996.
140 V. Valtchev and L. Tosheva, *Chem. Rev.*, 2013, **113**, 6734–6760.
141 M. Abbas, W. P. Lipiński, J. Wang and E. Spruijt, *Chem. Soc. Rev.*, 2021, **50**, 3690–3705.
142 T. P. Fraccia and N. Martin, *Nat. Commun.*, 2023, **14**, 2606.
143 P. G. Jamkhande, N. W. Ghule, A. H. Bamer and M. G. Kalaskar, *J. Drug Delivery Sci. Technol.*, 2019, **53**, 101174.

144 S. Shrestha, B. Wang and P. Dutta, *Adv. Colloid Interface Sci.*, 2020, **279**, 102162.
145 S. Franco-Ulloa, G. Tatulli, S. L. Bore, M. Moglianetti, P. P. Pompa, M. Cascella and M. De Vivo, *Nat. Commun.*, 2020, **11**, 5422.
146 J. Fei, J. Zhao, C. Du, A. Wang, H. Zhang, L. Dai and J. Li, *ACS Nano*, 2014, **8**, 8529–8536.
147 Z. Guo, J. Lu, W. Xie, X. Li, H. Wu and L. Zhao, *Mater. Chem. Phys.*, 2022, **281**, 125907.
148 G. Yun, S. Pan, T. Y. Wang, J. Guo, J. J. Richardson and F. Caruso, *Adv. Healthcare Mater.*, 2018, **7**, 1700934.
149 X. Zhang, X. Wang, M. Ning, P. Wang, W. Wang, X. Zhang, Z. Liu, Y. Zhang and S. Li, *Nanomaterials*, 2022, **12**, 2977.
150 X. Yu, T. J. Marks and A. Facchetti, *Nat. Mater.*, 2016, **15**, 383–396.
151 Y. Ren, Z. Ma and P. G. Bruce, *Chem. Soc. Rev.*, 2012, **41**, 4909–4927.
152 S. Choi, R. T. Rahman, B.-M. Kim, J. Kang, J. Kim, J. Shim and Y. S. Nam, *ACS Appl. Mater. Interfaces*, 2024, **16**, 16767–16777.
153 S. Pan, E. Goudeli, J. Chen, Z. Lin, Q. Z. Zhong, W. Zhang, H. Yu, R. Guo, J. J. Richardson and F. Caruso, *Angew. Chem., Int. Ed.*, 2021, **60**, 14586–14594.
154 X. Jia, J. Wu, K. Lu, Y. Li, X. Qiao, J. Kaelin, S. Lu, Y. Cheng, X. Wu and W. Qin, *J. Mater. Chem. A*, 2019, **7**, 14302–14308.
155 C. Park, B. J. Yang, K. B. Jeong, C. B. Kim, S. Lee and B.-C. Ku, *Angew. Chem., Int. Ed.*, 2017, **56**, 5485–5489.
156 T. W. Kim and K.-S. Choi, *Science*, 2014, **343**, 990–994.
157 Y. Shi, Y. Yu, Y. Yu, Y. Huang, B. Zhao and B. Zhang, *ACS Energy Lett.*, 2018, **3**, 1648–1654.
158 H. Sun, W. Hua, Y. Li and J.-G. Wang, *ACS Sustainable Chem. Eng.*, 2020, **8**, 12637–12645.
159 T. Tian, C. Dong, X. Liang, M. Yue and Y. Ding, *J. Catal.*, 2019, **377**, 684–691.
160 M. Lima, J. Avó, M. N. M. S. Berberan-Santos and C. I. C. Crucho, *ACS Appl. Nano Mater.*, 2022, **5**, 9460–9468.
161 C. Coll, A. Bernardos, R. Martínez-Máñez and F. Sancenón, *Acc. Chem. Res.*, 2013, **46**, 339–349.
162 S. M. Douglas, I. Bachelet and G. M. Church, *Science*, 2012, **335**, 831–834.
163 G. Fan, P. Wasuwanich, M. R. Rodriguez-Otero and A. L. Furst, *J. Am. Chem. Soc.*, 2021, **144**, 2438–2443.
164 G. Fan, J. Cottet, M. R. Rodriguez-Otero, P. Wasuwanich and A. L. Furst, *ACS Appl. Bio Mater.*, 2022, **5**, 4687–4695.
165 P. Wasuwanich, G. Fan, B. Burke and A. L. Furst, *J. Mater. Chem. B*, 2022, **10**, 7600–7606.
166 J. H. Park, K. Kim, J. Lee, J. Y. Choi, D. Hong, S. H. Yang, F. Caruso, Y. Lee and I. S. Choi, *Angew. Chem., Int. Ed.*, 2014, **53**, 12420–12425.
167 J. Pan, G. Gong, Q. Wang, J. Shang, Y. He, C. Catania, D. Birnbaum, Y. Li, Z. Jia, Y. Zhang, N. S. Joshi and J. Guo, *Nat. Commun.*, 2022, **13**, 2117.
168 X. Li, H. Liu, Z. Lin, J. J. Richardson, W. Xie, F. Chen, W. Lin, F. Caruso, J. Zhou and B. Liu, *Adv. Sci.*, 2024, **11**, 2308026.
169 H. Liu, S. Yu, B. Liu, S. Xiang, M. Jiang, F. Yang, W. Tan, J. Zhou, M. Xiao, X. Li, J. J. Richardson, W. Lin and J. Zhou, *Adv. Mater.*, 2024, **36**, 2401172.
170 N. K. Mandsberg, W. Liao, Y. A. Yamanouchi, A. Boisen and H. Ejima, *Algal Res.*, 2022, **61**, 102569.
171 J. Y. Oh, Y. Jung, Y. S. Cho, J. Choi, J. H. Youk, N. Fechler, S. J. Yang and C. R. Park, *ChemSusChem*, 2017, **10**, 1675–1682.
172 Y. Long, L. Xiao, Q. Cao, X. Shi and Y. Wang, *Chem. Commun.*, 2017, **53**, 10831–10834.
173 Y. Chen, Y. Bai, L. Meng, W. Zhang, J. Xia, Z. Xu, R. Sun, Y. Lv and T. Liu, *Chem. Eng. J.*, 2022, **437**, 135289.
174 T. Kitao, Y. Zhang, S. Kitagawa, B. Wang and T. Uemura, *Chem. Soc. Rev.*, 2017, **46**, 3108–3133.
175 J. Liang, S. Gao, J. Liu, M. Y. Zulkifli, J. Xu, J. Scott, V. Chen, J. Shi, A. Rawal and K. Liang, *Angew. Chem., Int. Ed.*, 2021, **60**, 5421.
176 R. Wang, X. Zhao, N. Jia, L. Cheng, L. Liu and C. Gao, *ACS Appl. Mater. Interfaces*, 2020, **12**, 10000–10008.
177 S. Dang, Q.-L. Zhu and Q. Xu, *Nat. Rev. Mater.*, 2017, **3**, 17075.
178 X. Zhang, Z. Chen, X. Liu, S. L. Hanna, X. Wang, R. Taheri-Ledari, A. Maleki, P. Li and O. K. Farha, *Chem. Soc. Rev.*, 2020, **49**, 7406–7427.
179 Z. Zheng, C. Borgs, J. T. Chayes and O. M. Yaghi, *J. Am. Chem. Soc.*, 2023, **145**, 18048–18062.

